Enhancement of Both Long-Term Depression Induction and Optokinetic Response Adaptation in Mice Lacking Delphilin

Tomonori Takeuchi[1☯], Gen Ohtsuki[2☯¤a], Takashi Yoshida[2☯¤b], Masahiro Fukaya[3], Tasuku Wainai[1¤c], Manami Yamashita[2], Yoshito Yamazaki[2], Hisashi Mori[1¤d], Kenji Sakimura[4], Susumu Kawamoto[5], Masahiko Watanabe[3], Tomoo Hirano[2*], Masayoshi Mishina[1*]

1 Department of Molecular Neurobiology and Pharmacology, Graduate School of Medicine, University of Tokyo, Tokyo, Japan, 2 Department of Biophysics, Graduate School of Science, Kyoto University, and CREST, Japan Science and Technology Agency, Kyoto, Japan, 3 Department of Anatomy, Hokkaido University School of Medicine, Sapporo, Japan, 4 Department of Cellular Neurobiology, Brain Research Institute, Niigata University, Niigata, Japan, 5 Department of Molecular Function, Research Center for Pathogenic Fungi and Microbial Toxicoses, Chiba University, Chiba, Japan

Abstract

In the cerebellum, Delphilin is expressed selectively in Purkinje cells (PCs) and is localized exclusively at parallel fiber (PF) synapses, where it interacts with glutamate receptor (GluR) δ2 that is essential for long-term depression (LTD), motor learning and cerebellar wiring. Delphilin ablation exerted little effect on the synaptic localization of GluRδ2. There were no detectable abnormalities in cerebellar histology, PC cytology and PC synapse formation in contrast to GluRδ2 mutant mice. However, LTD induction was facilitated at PF-PC synapses in Delphilin mutant mice. Intracellular Ca^{2+} required for the induction of LTD appeared to be reduced in the mutant mice, while Ca^{2+} influx through voltage-gated Ca^{2+} channels and metabotropic GluR1-mediated slow synaptic response were similar between wild-type and mutant mice. We further showed that the gain-increase adaptation of the optokinetic response (OKR) was enhanced in the mutant mice. These findings are compatible with the idea that LTD induction at PF-PC synapses is a crucial rate-limiting step in OKR gain-increase adaptation, a simple form of motor learning. As exemplified in this study, enhancing synaptic plasticity at a specific synaptic site of a neural network is a useful approach to understanding the roles of multiple plasticity mechanisms at various cerebellar synapses in motor control and learning.

Citation: Takeuchi T, Ohtsuki G, Yoshida T, Fukaya M, Wainai T, et al. (2008) Enhancement of Both Long-Term Depression Induction and Optokinetic Response Adaptation in Mice Lacking Delphilin. PLoS ONE 3(5): e2297. doi:10.1371/journal.pone.0002297

Editor: Seth G. N. Grant, Wellcome Trust Sanger Institute, United Kingdom

Received April 7, 2008; **Accepted** April 21, 2008; **Published** May 28, 2008

Funding: This work was supported by Grant-in-Aid for Scientific Research on Priority Areas-Molecular Brain Science from the Ministry of Education, Culture, Sports, Science and Technology of Japan, and the Japan Science and Technology Agency. G.O. and T.Y. were supported by Japan Society for the Promotion of Science.

Competing Interests: The authors have declared that no competing interests exist.

* E-mail: thirano@neurosci.biophys.kyoto-u.ac.jp (TH); mishina@m.u-tokyo.ac.jp (MM)

¤a Current address: Department of Neuroscience, Erasmus MC, Rotterdam, The Netherlands
¤b Current address: Department of Psychology, Brandeis University, Waltham, Massachusetts, United States of America
¤c Current address: Department of Anesthesiology and Critical Care Medicine, Omiya Medical Center, Jichi Medical School, Saitama, Japan
¤d Current address: Department of Molecular Neuroscience, Graduate School of Medicine, University of Toyama, Toyama, Japan

☯ These authors contributed equally to this work.

Introduction

Various studies suggest the important roles of the cerebellum in the regulation of fine motor control and motor learning [1,2]. The pattern of intrinsic neural connections in the cerebellum is known in considerable detail [3]. The wealth of knowledge of neural circuits in the cerebellum has led to the construction of models and theories of cerebellar functions [4–6]. These make the cerebellum an ideal system for studying the molecular and cellular mechanisms of brain function. The *N*-methyl-D-aspartate (NMDA) type of the glutamate receptor (GluR), a key molecule of synaptic plasticity and learning in the hippocampus and other forebrain regions, is absent in the cerebellar Purkinje cells (PCs). We found the δ subfamily of GluR by molecular cloning [7] and the second member of this subfamily, GluRδ2, is selectively expressed in cerebellar PCs [8,9]. In PCs, GluRδ2 is exclusively localized at parallel fiber (PF)-PC synapses [10,11]. Long-term depression (LTD) at PF-PC synapses, motor learning and motor coordination are impaired in GluRδ2 mutant mice [12–15]. In addition, a significant number of PC spines lack synaptic contacts with PF terminals and multiple climbing fiber (CF) innervation to PCs is sustained in GluRδ2 mutant mice [13,16–18]. Furthermore, inducible ablation of GluRδ2 in the adult brain causes mismatching and disconnection of PF-PC synapses [19]. Thus, GluRδ2 plays a central role in the synaptic plasticity, motor learning and neural wiring of cerebellar PCs. There is no evidence for GluRδ2 channel activities, although lurcher mutation transformed GluRδ2 to constitutively active channels [20]. One possible signaling mechanism through GluRδ2 is by protein-protein interactions. Truncation of the carboxyl-terminal PSD-95/Discs large/zona occludens-1 (PDZ)-binding domain of GluRδ2 (T site) impairs LTD induction at PF-PC synapses and caused CF territory expansion, but had little effect on

PF-PC synapse formation and elimination of surplus CFs at proximal dendrites of PCs [21]. Among PDZ proteins interacting with GluRδ2 at the T site, Delphilin appears to be interesting because of its selective expression in PCs except for a slight expression in the thalamus [22]. Within PCs, Delphilin is localized at PF synapses, but not at CF synapses. The characteristic expression pattern of Delphilin is reminiscent of GluRδ2. Here we report that Delphilin ablation results in the enhancement of both LTD induction at PF-PC synapses and optokinetic response (OKR) gain-increase adaptation, without affecting any detectable histological abnormalities. The phenotypes of Delphilin mutant mice are consistent with the idea that LTD induction at PF-PC synapses is a crucial rate-limiting step in OKR gain-increase adaptation, a simple form of motor learning.

Methods

Generation of Delphilin mutant mice

We isolated a mouse genomic clone carrying exon 2 and 3 of the *Delphilin* gene by screening a bacterial artificial chromosome library prepared from the C57BL/6 strain (Incyte Genomics, St. Louis, MO). The 34-bp *loxP* and 16-bp linker sequences were inserted into the *Avr*II site 93-bp upstream of exon 2, and the 1.9-kb DNA fragment carrying the 34-bp *loxP* sequence and *Pgk-1* promoter-driven *neo* gene flanked by two *frt* sites into the *Sph*I site 423-bp downstream of exon 3. Targeting vector pTVDEL1 contained exon 2 and 3 of the *Delphilin* gene flanked by *loxP* sequences, the 6.7-kb upstream and 2.3-kb downstream genomic sequences and 4.3-kb pMC1DTpA [23]. Homologous recombination in C57BL/6 embryonic stem cells and chimeric mouse production were carried out as described previously [19]. A chimeric mouse with the floxed *Delphilin* gene was mated to TLCN-Cre mice [24,25], which were backcrossed 5 times to the C57BL/6 strain, to yield $Del^{+/-}$ mice. The *cre* gene was bred out and heterozygous Delphilin mutant mice were crossed with each other. Resulting homozygous mutant mice ($Del^{-/-}$) and wild-type littermates ($Del^{+/+}$) were used as mutant and control mice, respectively. The wild-type and mutant mice of 9 to 10 weeks old were used for subsequent analyses unless otherwise specified. The genotypes of mice were determined by polymerase chain reaction using primers 5′-GCTGGGAATGCAAGTCTGTT-3′ (DelP1), 5′-TGCGACACCACCTCGTCGAA-3′ (DelP2), and 5′-CTGACTAGGGGAGGAGTAGA-3′ (NeoR). Mice were fed *ad libitum* with standard laboratory chow and water in standard animal cages under a 12-h light: 12-h dark cycle. All animal procedures were approved by the Animal Care and the Use Committee of Graduate School of Medicine, the University of Tokyo (Approval # 1721T062), the Local Committee for Handling Experimental Animals in the Graduate School of Science, Kyoto University (Approval # H1804-12 and H1804-13), and the Animal Care and Use Committee of Hokkaido University (Approval # 06012).

Western blot analysis

Whole homogenates were prepared from cerebella of mice at postnatal day 42 (P42) as described [26]. Western blot analysis was carried out as described [19]. Primary antibodies were guinea pig anti-Delphilin [22], rabbit anti-GluR2/3 (Upstate, Charlottesville, VA), rabbit anti-GluRδ2 [8], rabbit anti-postsynaptic density (PSD)-93 [27], rabbit anti-PTPMEG [28], rabbit anti-Synapsin I (Merck, Darmstadt, Germany) and rabbit anti-neuron specific enolase (NSE) [29]. Expression levels in the mutant mice were estimated as percentages of those in the wild-type mice using NSE as an internal standard.

Histological analyses

Histological and electron microscopic analyses were carried out as described [19,30]. Immunoperoxidase staining was carried out using guinea pig anti-Delphilin antibody. Double immunofluorescence was carried out using rabbit anti-calbindin [31], guinea pig anti-vesicular glutamate transporter 1 (VGluT1), guinea pig anti-vesicular glutamate transporter 2 (VGluT2), and rabbit anti-vesicular γ-amino butyric acid transporter (VGAT) [32] antibodies. To count PF-PC synapses on electron micrographs, 20 electron micrographs were taken randomly for each mouse from the molecular layer in the lobule IV/V at an original magnification of ×4,000 with an H-7100 electron microscope (Hitachi High-Technologies, Tokyo, Japan). Post-embedding immunogold analysis was carried out as described [22,30] using rabbit anti-GluRδ2 antibody or the mixture of rabbit anti-GluR1, GluR2 and GluR3 antibodies [33].

Electrophysiological analyses

Parasagittal cerebellar slices (250-μm thickness) were prepared from mice at P14-P18 unless otherwise stated. Whole-cell voltage-clamp recordings were performed on PCs in the II-VIII lobules of vermal region. A PC was whole-cell voltage-clamped with a patch pipette (2–3 MΩ) filled with the internal solution consisting of (in mM) 150 CsCl, 0.5 EGTA, 9 sucrose, 10 HEPES, 2 Mg-ATP (Sigma-Aldrich, St. Louis, MO) and 0.2 Na-GTP (Sigma-Aldrich), titrated to pH 7.3 with CsOH unless otherwise stated. The slices were continuously perfused with the oxygenated Krebs' solution containing (in mM) 124 NaCl, 1.8 KCl, 1.24 KH_2PO_4, 1.3 $MgCl_2$, 2.5 $CaCl_2$, 26 $NaHCO_3$ and 10 glucose with 95% O_2 and 5% CO_2 at 22–24°C. Bicuculline (20 μM, Sigma-Aldrich) was added to suppress spontaneous inhibitory postsynaptic currents. Ionic currents were recorded with an EPC-9 or an EPC-10 amplifier (HEKA Elektronik, Lambrecht, Germany), and the signal was filtered at 1.5 or 2.9 kHz and digitized at 10 kHz. The membrane potential was held at −80 mV after compensation of the liquid junction potential unless otherwise stated.

To record miniature excitatory postsynaptic currents (mEPSCs), 1 μM tetrodotoxin (Wako Pure Chemical, Osaka, Japan) was applied to prevent action potential (AP) generation. The mean amplitude of mEPSC in a particular neuron was calculated from more than 300 mEPSCs, and the mean±SEM from 20 neurons are presented. The 10–90% rise time and the half-height width were measured in 10–11 mEPSCs in a PC and averaged, and the mean±SEM among 10 PCs was calculated. The metabotropic glutamate receptor type 1 (mGluR1)-mediated slow synaptic response was induced by repetitive stimulation of PFs (50 Hz, 1–20 times) in the molecular layer in the presence of 10 μM α-amino-3-hydroxy-5-methyl-4-isoxazolepropionic acid (AMPA) receptor blocker 2,3-dioxo-6-nitro-1,2,3,4-tetrahydrobenzo[f]quinoxaline-7-sulfonamide (NBQX) (Tocris Cookson, Bristol, UK) in addition to bicuculline. The CF response was induced by applying electrical stimulation (200 μs) to the granular layer near the soma of PC prepared from P22-P24 mice voltage clamped at −20 mV. In order to estimate the number of CF innervations, the intensity of stimulation was gradually increased from 0 V to 50 V by 3–5 V, and the number of amplitude steps in EPSCs was counted. It is known that most PCs are innervated by single CF at P22-P24. The Ca^{2+} current through voltage-gated Ca^{2+} channels was recorded by applying 20 ms depolarizing voltage pulses to a PC prepared from a P5 mouse in the presence of 10 mM tetraethylammonium chloride (Sigma-Aldrich), 1 mM 4-aminopyridine (Sigma-Aldrich) and 1 μM tetrodotoxin in addition to bicuculline and NBQX. Immature PCs were used in the Ca^{2+} current measurement to obtain a better voltage- and space-clamp

condition. The series resistance compensation was optimized for Ca^{2+} current recording. The resting potential and AP were also recorded under the current-clamp condition with the K-gluconate internal solution in which CsCl and CsOH were replaced with K-gluconate and KOH, respectively. The series resistance compensation was optimized. PC firing frequency was measured under the cell-attached or current-clamp condition.

To monitor LTD, test pulses (1–10 V, 200 μs) were applied to PFs in the molecular layer at 0.05 Hz, except for the period of conjunctive stimulation. The intensity of stimulus was adjusted to evoke PF-EPSC whose initial amplitude was 100–200 pA. After stable recording for at least 7.5 min, the conditioning stimulation was applied to induce LTD. The conditioning stimulation was 200 ms depolarization of a PC to −20 mV coupled with the paired PF stimuli applied at 15 and 65 ms after the onset of depolarization. This conjunctive stimulation was repeated once, twice, 5 times, 10 times or 20 times at 1 Hz. In some experiments, 10 mM EGTA was added to the internal solution. Series resistance (10–30 MΩ) and input resistance were monitored every 2.5 min by applying a +10 mV, 80 ms voltage pulse to −70 mV. The data were discarded if the series resistance changed by more than 20% or the input resistance became <100 MΩ.

OKR recordings

Eye movement recordings were performed by the video method as described [34,35]. The sampling frequency of the image was 30 Hz. To induce OKR the screen with vertical black and white stripes (14°) that surrounds a mouse was rotated sinusoidally in light. The traces of eye velocity calculated from eye positions, and the stimulus (screen or turntable rotation) velocity were fitted with the respective sine curves by a least square method for at least successive 10 cycles except for the recording at 0.1 Hz (5 cycles or more). The gain of OKR was defined as the amplitude of fitted sine curve of eye velocity divided by that of stimulus. The negative value in phase indicates the lead of eye movement relative to the stimuli, and the positive value indicates the lag. Dynamic properties of OKR were measured twice and averaged values were used for the data analysis. To induce the adaptive change in OKR, the surrounding screen was rotated sinusoidally at 0.2 Hz, ±7.2° for 60 min each day. To prevent extinction of the learned response, the animals were kept in the dark between sessions. During the training paradigms, we made noises by clapping hands every 5 min in order to keep a mouse in an aroused state.

Motor coordination test

Naive male mice were housed individually and were handled for ~1 min a day for 7–10 days before behavioral tests. An animal was placed in the midpoint of a thin rod (TR-3002; O'Hara, Tokyo, Japan), and given six trials with 30-min inter-trial intervals. For a rotarod test, mice were habituated to an apparatus (RRSW-3002, O'Hara) by placing them on the rod rotating at 2.5 rpm (3×2 min sessions). An animal was placed on the rod rotating at 25 rpm, and given three trials with 45- to 60-min inter-trial intervals for 4 consecutive days.

Statistical analyses

All behavioral experiments were performed in a blind fashion. Data were expressed as mean±SEM. Statistical analysis was performed using Student's *t* test, Mann–Whitney *U* test, Fisher's exact probability test or ANOVA with repeated measures as appropriate. Correlation analysis was done using Pearson's coefficient of comparison. Statistical significance was set at $p<0.05$.

Results

Cerebellar structure of mutant mice lacking Delphilin

To examine the functional role of Delphilin in the cerebellum, we generated mutant mice lacking Delphilin (Fig. 1A). The Delphilin mutant mice grew and mated normally. Western blot analysis confirmed the absence of Delphilin of 135 kDa in the mutant mice (Fig. 1B). Strong immunohistochemical signals of Delphilin in the cerebellar molecular layer as well as faint signals in the thalamus attenuated in the mutant mice (Fig. 1C).

The cerebellum of the mutant mice exhibited normal foliation and laminated cortical structures (Fig. 1D). Double immunostaining for calbindin and VGluT1 revealed that PCs extended well-arborized dendrites studded with numerous spines (Fig. 1E,F), which were tightly associated with PF terminals (Fig. 1I,J). Immunostaining for VGluT2 and VGAT showed that the innervation patterns of CF and inhibitory terminals in the cerebellar molecular layer were comparable between the wild-type and mutant mice (Fig. 1G,H). In both genotypes, PC spines forming asymmetrical synapses were distributed in large numbers in the neuropil of the molecular layer (Fig. 1I,J). The cytoarchitecture and synaptic differentiation in the flocculus and paraflocculus were also indistinguishable between the wild-type and mutant mice (Fig. S1). The numbers of PF-PC synapses per 100 μm^2 of the neuropil area were comparable between the wild-type (20.9±1.0, mean±SEM, n = 4) and mutant mice (20.7±0.5, n = 6; Mann–Whitney *U* test, $p>0.05$). Thus, Delphilin ablation exerted little effect on cerebellar histology, PC cytology and PC synapse formation.

Expression and localization of GluRδ2

Immunoblot analyses of the whole cerebellar homogenates showed that the amounts of GluRδ2 as well as PSD-93, PTPMEG and Synapsin I were comparable between the wild-type and mutant mice (n = 3 for each; Student's *t* test, $p>0.2$ in all cases), while those of anti-GluR2/3 antibody-immunoreactive AMPA receptor proteins were slightly increased in the mutant mice ($p = 0.005$, Fig. 2A). Both Delphilin and GluRδ2 are selectively localized at PF-PC synapses and interact with each other [13,22]. We thus examined the effect of Delphilin ablation on the synaptic localization of GluRδ2 by the postembedding immunogold technique. In both genotypes, immunogold labeling of GluRδ2 was concentrated at PF-PC synapses (Fig. 2B). GluRδ2-particles were hardly found at CF-PC and interneuron (IN)-PC synapses (Fig. 2C). No significant differences were detected in labeling density between the wild-type and mutant mice in each type of PC synapses (Mann–Whitney *U* test, $p>0.4$ in all cases). In the perpendicular synaptic localization, gold particles for GluRδ2 peaked at 0–8 nm bin just postsynaptic from the midpoint of the postsynaptic membrane in both mice (Fig. 2D). In the tangential synaptic localization, gold particles were deposited uniformly along the postsynaptic membrane, except for the marginal 20% (80–100% bin) that showed a slight reduction (Fig. 2E). These results suggest that Delphilin ablation exerted little effect on the synaptic localization of GluRδ2. The synaptic distribution of AMPA receptors was also examined by the postembedding immunogold technique. Gold particles representing AMPA receptors were detected on the postsynaptic membrane of PF-PC synapses in both genotypes (Fig. 2F). When quantified, the number of gold particles of AMPA receptors per profile of PF-PC synapses in the mutant mice (6.4±0.3, n = 300 from 3 mice) was significantly larger than that in the wild-type mice (4.6±0.3, n = 300 from 3 mice; Mann–Whitney *U* test, $p<0.001$).

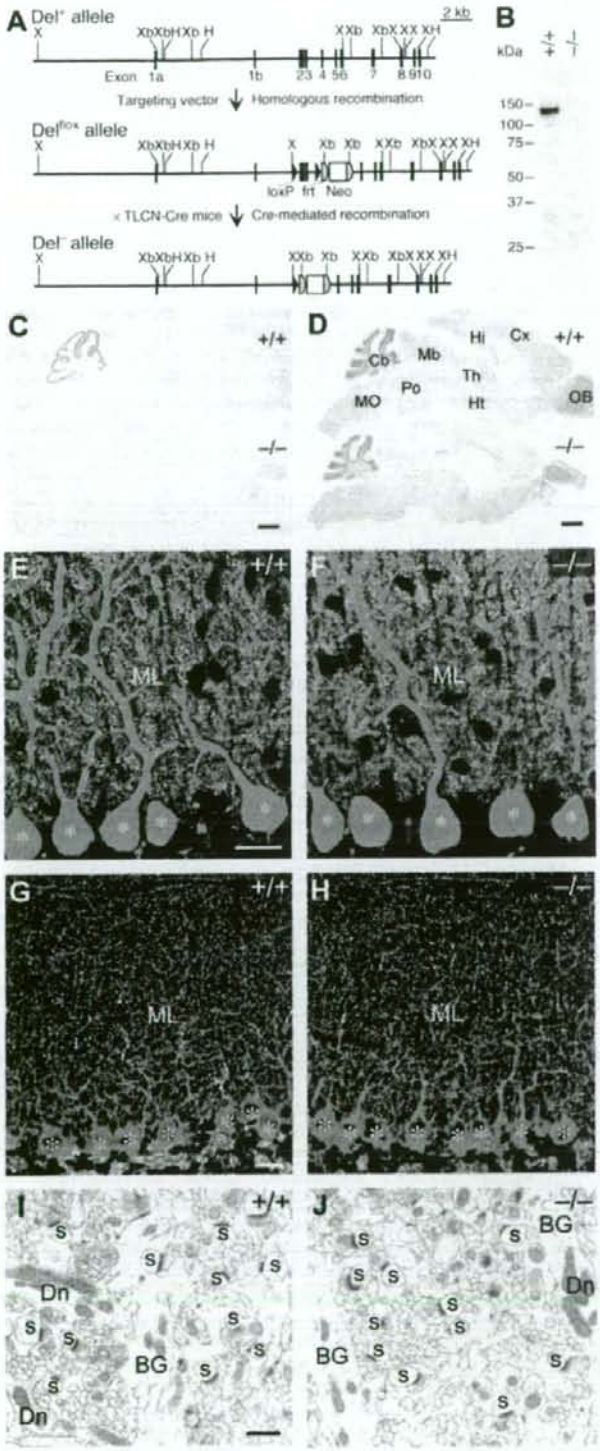
A
Del+ allele
2 kb
Exon 1a
1b
Targeting vector
Homologous recombination
Delflox allele
loxP frt Neo
× TLCN-Cre mice
Cre-mediated recombination
Del− allele
B
kDa
150–
100–
75–
50–
37–
25–
C
+/+
–/–
D
Hi
Cx
Cb
Mb
Th
Po
MO
Ht
OB
E
F
G
H
ML
I
J
Dn
BG
s

Figure 1. Generation and cerebellar structure of mutant mice lacking Delphilin. A, Schema of the *Delphilin* gene (*Del*$^{+}$), floxed allele (*Del*^{flox}), and null allele (*Del*$^{-}$). Exon 3 encodes the PDZ domain of Delphilin. The *Del*^{flox} allele contains two *loxP* sequences flanking exon 2 and 3 of the *Delphilin* gene and the *neo* gene flanked by two *frt* sequences. *Del*$^{+/-}$ mice were obtained by crossing *Del*$^{+/flox}$ mice with TLCN-Cre mice. Neo, neomycin phosphotransferase gene; H, *Hin*cII; X, *Xho*I, Xb, *Xba*I. **B**, Western blot analysis of Delphilin in cerebellar homogenates. **C**, Immunohistochemical analysis of Delphilin in the parasagittal brain sections. **D**, Hematoxylin staining of the parasagittal brain sections. Cb, cerebellum; Cx, Cerebral cortex; Hi, hippocampus; Ht, hypothalamus; Mb, midbrain; MO, medulla oblongata; OB, olfactory bulb; Po, pons; Th, thalamus. **E,F**, Double immunofluorescence for calbindin (green) and VGluT1 (red) in the cerebellar molecular layer of wild-type (**E**) and mutant (**F**) mice. Asterisks indicate the cell body of PCs. ML, molecular layer. **G,H**, Double immunofluorescence for VGAT (green) and VGluT2 (red) in the cerebellar molecular layer of wild-type (**G**) and mutant (**H**) mice. Asterisks indicate the cell body of PCs. ML, molecular layer. **I,J**, Electron micrographs of the cerebellar molecular layer of wild-type (**I**) and mutant (**J**) mice. BG, Bergmann glia; Dn, PC dendrite; s, PC spine in contact with PF terminals. Scale bars: **C,D**, 1 mm; **E,G**, 20 μm; **I**, 1 μm.
doi:10.1371/journal.pone.0002297.g001

Facilitation of LTD induction

There were no significant differences between the wild-type and mutant PCs in basal electrical properties including input resistance, resting potential, AP firing frequency, amplitude, threshold and half-height width (Table 1). The amplitude of mEPSCs was slightly larger in the mutant mice; however, the frequency and time course of mEPSCs were not significantly different between the genotypes (Table 1).

In cerebellar slices of both genotypes, 10 paired-stimulations of PFs in conjunction with PC depolarization induced robust LTD (Fig. 3A). The amplitude of LTD measured 30 min after the induction in the mutant mice (52.5±13.7%, n = 7) was comparable to that in the wild-type mice (56.0±5.0%, n = 7; Student's *t* test, p = 0.82). The 5 conjunctions induced weak LTD in the wild-type mice (87.5±13.9%, n = 6). In contrast, robust LTD was induced in the mutant mice (47.8±14.9%, n = 6; p = 0.02; Fig. 3B). Further, 2 conjunctions failed to induce LTD in the wild-type mice (97.3±12.1%, n = 7). However, this weak conditioning successfully induced robust LTD in the mutant mice (55.0±5.4%, n = 10; p = 0.01; Fig. 3C). The amplitudes of LTD induced by the 2-conjunction stimulation in the mutant mice were comparable to those induced by the 10-conjunction stimulation in the wild-type or mutant mice (p = 0.90 and 0.87, respectively; Fig. 3E). Just one conjunction induced weak LTD in the mutant mice (78.9±8.3%, n = 6) but not in the wild-type mice (101.5±18.8%, n = 5; p = 0.28; Fig. 3D). These results do not necessarily mean that LTD can be induced by a single or a few conjunctions of CF and PF activities *in vivo*, because in the present experiments Cs^{+} was introduced into a PC that should have enhanced the Ca^{2+} influx. However, they suggest that LTD is induced relatively easily in the mutant mice *in vivo*. The time courses of LTD development (decrease in PF-EPSC amplitude) were similar irrespective of the number of conditioning conjunctions in both the wild-type and mutant mice. Together, these results suggest that Delphilin ablation facilitated LTD induction at PF-PC synapses with little effect on the saturation level of the amplitude.

Ca^{2+} influx through voltage-gated Ca^{2+} channels, mGluR1 activation and AMPA receptor activation are required to induce LTD [36,37]. The amplitudes of Ca^{2+} influx through voltage-gated Ca^{2+} channels for the two genotypes were similar (Table 1). A repetitive stimulation of PFs induces a slow inward current mediated by mGluR1 [38]. No significant difference was detected between the wild-type and mutant mice in terms of the amplitude and time course of the mGluR1-mediated slow synaptic response (Fig. 4A, Table 1). Cytosolic Ca^{2+} is necessary to induce LTD at PF-PC synapses [37]. When 10 mM EGTA was introduced into a PC, LTD was strongly suppressed in the wild-type mice (95.1±9.4%, n = 5) but only weakly in the mutant mice (63.1±7.2%, n = 5; Student's *t* test, p = 0.03; Fig. 4B). These results suggest that LTD was induced with less intracellular Ca^{2+} in the mutant mice.

CF responses were recorded from P22-P24 mice, and the number of amplitude steps of EPSCs in response to the stimulation whose intensity was gradually increased was determined. CF responses with multiple amplitudes were limited in both genotypes (wild-type, 2 of 22; mutant, 2 of 17; Fig. 5A). This indicates that multiple innervations of CFs were rare in the mutant mice as in the wild-type mice (Fisher's exact probability test, p = 0.59). The amplitudes and time course of CF-EPSCs were also similar in the two genotypes (Student's *t* test, p>0.6 in all cases; Fig. 5B,C).

Enhancement of OKR adaptation

To test the learning ability of Delphilin mutant mice, we examined OKR, the eye movement that follows the movements of large visual fields, and its adaptation. The cerebellar flocculus is involved in OKR adaptation, while vestibular nuclei play a central role in OKR [6]. OKR was elicited by sinusoidally oscillating a vertically striped screen surrounding an animal at 0.1–1.6 Hz, ±1.8–14.4° in light. The gain, which is the relative amplitude of eye movement against screen movement and the phase, which is the delay of eye movement from screen movement, were analyzed. The OKR gains of the wild-type and mutant mice decreased as the frequency of screen oscillation was increased at a fixed peak amplitude of 1.8° and as the angular amplitude of screen oscillation was increased at a fixed frequency of 0.4 Hz (Fig. 6A). Under these conditions, the mutant mice showed a slightly larger OKR gain than the wild-type mice (ANOVA with repeated measures, genotype effect, $F_{(1,25)} = 6.0$, p = 0.02). The OKR phase lags were less than 20° except at a frequency of 1.6 Hz (Fig. 6B). There were no significant differences in OKR phase lag between the two genotypes (genotype effect, $F_{(1,23)} = 2.2$, p = 0.15).

Continuous oscillation of the screen at 0.2 Hz, ±7.2° for 60 min induced an increase in OKR gains in both the wild-type and mutant mice (Fig. 6C,D). The adaptive increase in OKR gain in the mutant mice was significantly larger than that in the wild-type mice (genotype effect, $F_{(1,23)} = 10.2$, p = 0.004). The difference in basal OKR gain might have affected the learning process. However, there was no significant correlation between the basal OKR gain and the adaptive increase in OKR gain in each genotype (Pearson: wild-type, r = −0.30, p = 0.42; mutant, r = 0.46, p = 0.09). The adaptive decreases of OKR phase lag were similar for two genotypes (ANOVA with repeated measures, genotype effect, $F_{(1,23)} = 0.35$, p = 0.56). When the training was conducted for 5 consecutive days, the OKR gains of both the wild-type and mutant mice increased significantly with the number of training sessions (session effect, $F_{(9,207)} = 82.1$, p<0.001; Fig. 6E). On days 1 to 4, the mutant mice showed significantly larger gains than the wild-type mice (genotype effect, p = 0.008-0.04). However, the OKR gains of the wild-type mice became comparable to those of the mutant mice on day 5 (genotype effect, $F_{(1,23)} = 0.28$, p = 0.60). The OKR phase lag decreased with the number of training sessions in both genotypes (session effect, $F_{(9,207)} = 25.8$, p<0.001; Fig. 6F). There were no significant differences in phase

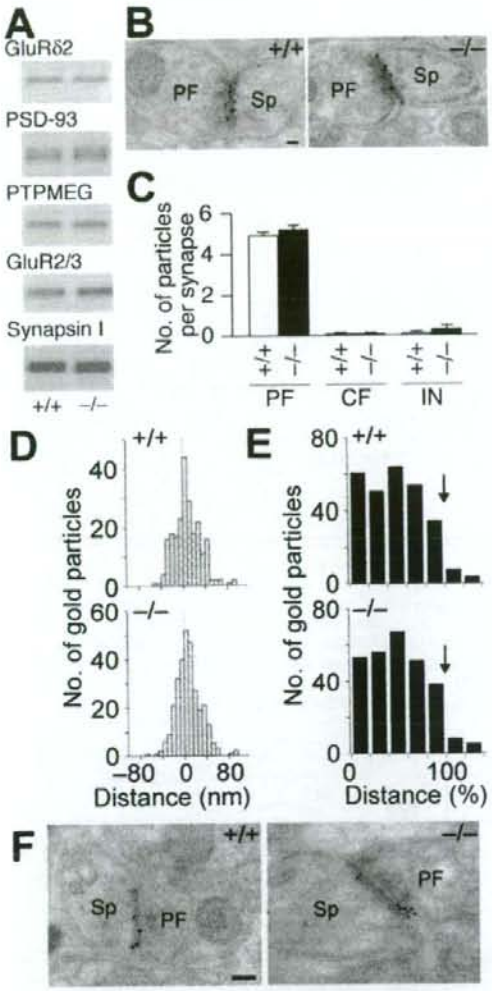

Figure 2. Expression and distribution of GluRδ2 at PF-PC synapses. **A**, Representative Western blots of GluRδ2, PSD-93, PTPMEG, GluR2/3 and Synapsin I in the cerebellum. **B**, Postembedding immunogold for GluRδ2 at PF-PC synapses. PF, parallel fiber; Sp, spine. **C**, The number of immunogold particles for GluRδ2 per profile of PF-PC synapses (+/+, n = 217; −/−, n = 179), CF-PC synapses (+/+, n = 12; −/−, n = 23) and IN-PC synapses (+/+, n = 9; −/−, n = 25). Data are expressed as mean± SEM. **D**, Perpendicular localization of GluRδ2 at PF-PC synapses. The distances from the midpoint of the postsynaptic membrane to the center of gold particles were grouped into 8-nm bins. **E**, Tangential localization of GluRδ2 at PF-PC synapses. The relative medio-lateral position of gold particles is indicated as the percentage of the distance from the center (0%) to the edge (100%) of the PSD. Arrows indicate the boundary of PSD. **F**, Postembedding immunogold for AMPA receptors at PF-PC synapses. PF, parallel fiber; Sp, spine. Scale bars: **B,F**, 100 nm.
doi:10.1371/journal.pone.0002297.g002

lag between the two genotypes throughout the 5 training days (genotype effect, p = 0.08–0.64). Thus, Delphilin ablation augmented the adaptive increase in OKR gain but not the adaptive decrease in OKR phase lag.

Finally, the motor coordination of the mutant mice was examined. In the thin rod test, the retention times on a thin stationary plexiglass rod for the wild-type and mutant mice were indistinguishable (ANOVA with repeated measures, genotype effect, $F_{(1,29)} = 0.002$, p = 0.96; Fig. 7A). No significant differences in the retention time were observed on the rotating rod at 25 rpm between the two genotypes (genotype effect, $F_{(1,40)} = 1.1$, p = 0.29; Fig. 7B).

Table 1. Basal electrical properties of PCs in wild-type and mutant mice

Properties	Wild-type	Mutant
Resting potential, mV	−63±1 (10)	−61±2 (8)
Action potential		
Frequency, Hz	28±2 (31)	26±2 (32)
Amplitude, mV	62±2 (10)	60±2 (8)
Half-height width, ms	0.8±0.1 (10)	0.8±0.1 (8)
Threshold, mV	−41±0.6 (10)	−41±1.3 (8)
Input resistance, MΩ	294±29 (12)	313±45 (10)
mEPSC		
Amplitude, pA	11.3±0.4 (20)	12.8±0.5 (20)
Frequency, Hz	4.1±0.7 (20)	3.2±0.3 (20)
Half-height width, ms	12.9±0.8 (10)	12.8±0.7 (10)
10–90% rise time, ms	2.6±0.2 (10)	2.7±0.2 (10)
mGluR response		
Amplitude, pA	123±9 (6)	113±9 (6)
Half-height width, ms	737±121 (6)	989±206 (6)
10–90% rise time, ms	171±14 (6)	218±29 (6)
Ca^{2+} current at 0 mV, nA	2.0±0.3 (6)	1.8±0.2 (6)

Data are expressed as mean±SEM. Numbers in parentheses indicate the number of neurons. mGluR1 mediated synaptic response was induced by 10 pulses. There were no significant differences between wild-type and mutant PCs in basal electrical properties (Student's *t* test, p>0.1 in all cases) except for the amplitude of mEPSC (p = 0.02).
doi:10.1371/journal.pone.0002297.t001

Discussion

Here, we showed that Delphilin ablation at PF-PC synapses facilitates LTD induction at PF synapses and enhances OKR gain-increase adaptation without affecting any detectable histological abnormalities. This finding is compatible with the idea that LTD induction at PF-PC synapses is a crucial rate-limiting step in OKR gain-increase adaptation, a simple form of motor learning.

Examination of LTD under various stimulation conditions revealed that Delphilin ablation facilitated LTD induction at PF-PC synapses. On the other hand, the saturation levels of LTD amplitude for the wild-type and mutant mice were comparable. The time courses of LTD development after different numbers of conditioning conjunctions were also similar in both genotypes, implying that LTD expression itself proceeds normally in the mutant mice. Cumulative studies suggest that GluRδ2, mGluR1, AMPA receptors and Ca^{2+} are key mediators of LTD induction [36,37]. However, Delphilin ablation appeared to exert little effect on the amount and localization of GluRδ2 and on the amplitude and kinetics of mGluR1-mediated slow synaptic responses. There were no significant differences between the wild-type and mutant PCs in basal electrical properties and the frequency and time course of mEPSCs although the amplitude of mEPSCs and the amount of AMPA receptors at PF-PC synapses were somewhat larger in the mutant mice. On the other hand, we observed that

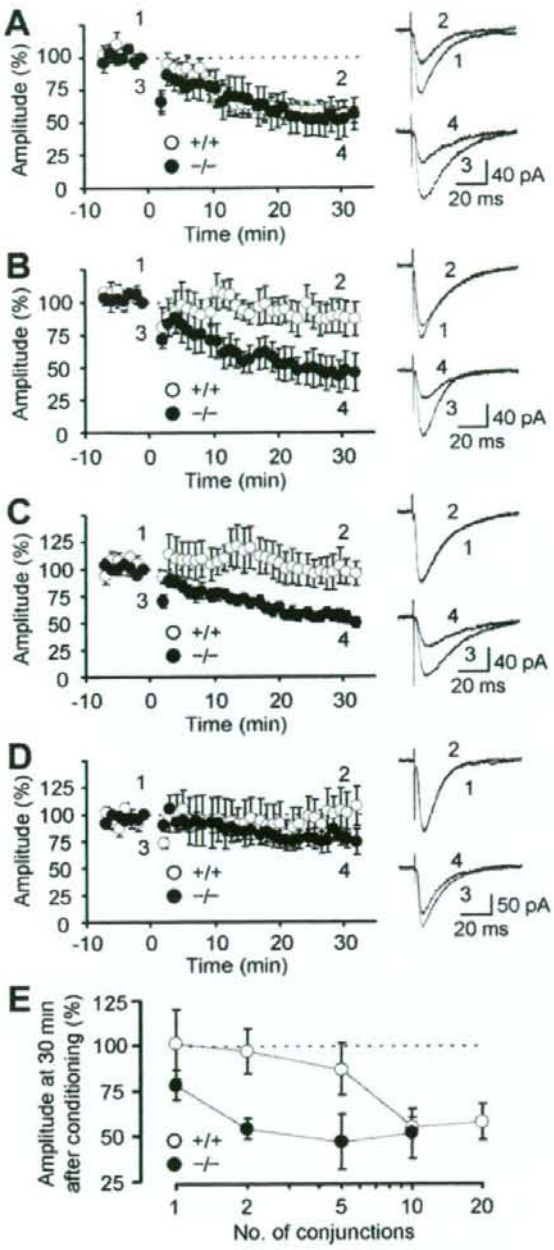

Figure 3. LTD at PF-PC synapses. A, Time courses of LTD at PF-PC synapses induced by 10-conjunction stimulation in wild-type and mutant mice. Representative PF-EPSCs recorded at the times indicated by numbers are shown on the right. The conditioning stimulation was applied at 0 min. The amplitude of PF-EPSC was normalized using the mean amplitude of EPSCs recorded for 1 min before the conditioning as the reference. **B**, Time courses of LTD induced by 5-conjunction stimulation. **C**, Time course of LTD induced by the 2 conjunctions. **D**, Time course of LTD induced by one conjunction. **E**, The percentile of depression 30 min after the conditionings was presented against the number of conjunctions. Data are expressed as mean±SEM.

doi:10.1371/journal.pone.0002297.g003

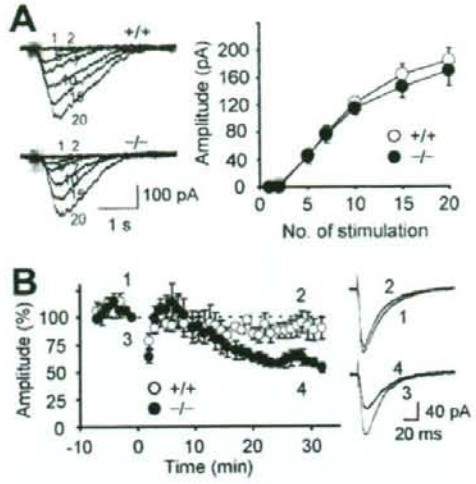

Figure 4. mGluR1-mediated synaptic response and effect of EGTA on LTD. A, mGluR1-mediated synaptic response induced in the presence of NBQX. PFs were repetitively (50 Hz, 1–20 pulses) stimulated. Representative traces and amplitudes of responses are presented. Each number beside traces represents the number of stimulation pulses. **B**, Time courses of LTD induced by 10-conjunction stimulation in PCs loaded with 10 mM EGTA. Representative PF-EPSCs recorded at the times indicated by numbers are shown on the right. The conditioning stimulation was applied at 0 min. Data are expressed as mean±SEM.

doi:10.1371/journal.pone.0002297.g004

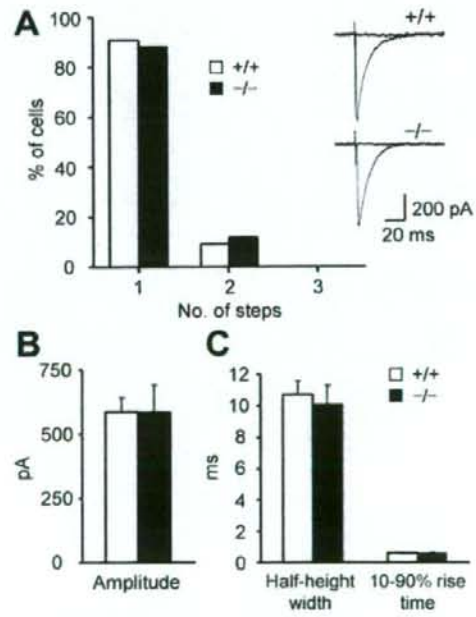

Figure 5. Synaptic responses at CF-PC synapses. A, The numbers of amplitude steps in CF-EPSCs (+/+, n = 22; −/−, n = 17). Representative CF-EPSCs are presented. **B,C**, The amplitude (**B**), half-height width and 10–90% rise time (**C**) of CF-EPSCs (+/+, n = 15; −/−, n = 10). Data are expressed as mean±SEM.

doi:10.1371/journal.pone.0002297.g005

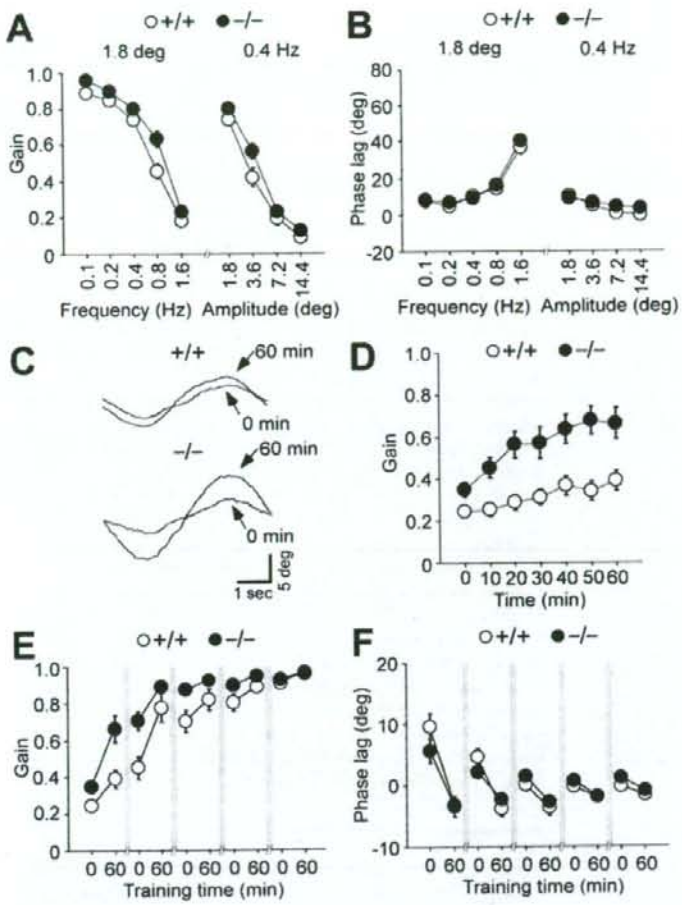

Figure 6. Dynamic properties and adaptive changes of OKR. A,B, Dynamic properties of OKR. The gain (**A**) and phase (**B**) values in wild-type (n = 14) and mutant (n = 13) male mice were measured during OKR. The peak amplitude of screen oscillation was fixed at 1.8°, or the frequency of screen oscillation was fixed at 0.4 Hz. **C–F**, Adaptive modification of OKR induced by a 60-min sustained sinusoidal screen oscillation at 0.2 Hz, ±7.2° in light over 5 days. Representative OKR traces before and after 60 min of sustained screen oscillation on day 1 (**C**). Changes in OKR gain during 60 min of sustained screen oscillation on day 1 in wild-type (n = 10) and mutant (n = 15) mice (**D**). Changes in OKR gain (**E**) and phase lag (**F**) over 5 days. There were rest periods for 23 h in the dark between training sessions as indicated by shaded bars. Data are expressed as mean±SEM.
doi:10.1371/journal.pone.0002297.g006

the Ca^{2+} requirement of LTD induction machinery was altered in the mutant mice, since 10 mM EGTA suppressed LTD strongly in the wild-type mice but only weakly in the mutant mice. The decreased dependence on the intracellular Ca^{2+} appears to be the main cause of the facilitation of LTD induction in the mutant mice.

Delphilin is distributed predominantly in cerebellar PCs and is localized selectively at PF synapses within PCs [22]. At PF-PC synapses, Delphilin binds to the carboxyl terminal of GluRδ2 that plays a central role in synaptic plasticity, motor learning and cerebellar wiring [13,19,39–41]. In contrast to the GluRδ2 mutant mice, the Delphilin mutant mice showed no detectable abnormalities in the cerebellar histology or morphology of PF synapses. In addition, Delphilin ablation exerted little effect on the expression and synaptic localization of GluRδ2. Consistently, the truncation of the PDZ-binding domain at the carboxyl terminal of GluRδ2 exerted little effect on the synaptic localization of receptor proteins, histological features and the fine structures of PF-PC synapses [21]. On the other hand, Delphilin ablation facilitated the induction of LTD, whereas LTD was impaired in the mutant mice carrying carboxyl-terminal truncated GluRδ2. It is likely that several domains for protein-protein interactions differentially mediate diverse GluRδ2 functions [19,21,42,43] and multiple PDZ proteins interacting with the carboxyl terminal of GluRδ2, such as Delphilin, PSD-93, PTPMEG, nPIST and S-SCAM [22,28,44–46], may positively or negatively regulate LTD by mediating different downstream signaling. In fact, LTD was impaired in PTPMEG mutant mice [47]. The facilitation of LTD at PF-PC synapses in Delphilin mutant mice is reminiscent of the enhanced long-term potentiation (LTP) at hippocampal CA3-CA1 synapses in PSD-95 and synapse-associated protein 102 (SAP102) mutant mice [48,49]. Delphilin, PSD-95 and SAP102 share similarities at the molecular levels–they are PSD proteins interacting with the carboxyl-terminal of glutamate receptors.

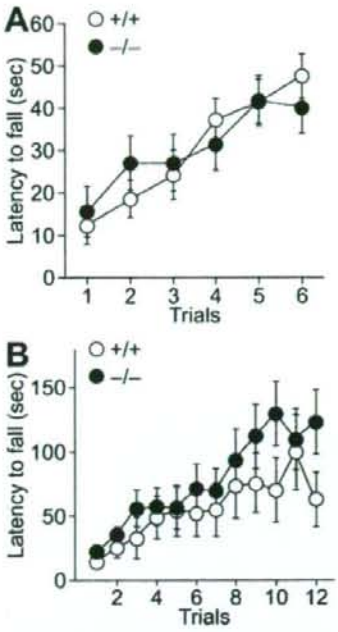

Figure 7. Motor coordination. A, The stationary horizontal thin rod test. Wild-type (n = 17) and mutant (n = 14) male mice were placed on the stationary horizontal thin rod and the time each mouse remained on the rod was measured. **B**, The rotating rod test. Rotarod performance of wild-type (n = 18) and mutant (n = 24) male mice. Retention time on the rotating rod at 25 rpm was measured. Data are expressed as mean ± SEM.
doi:10.1371/journal.pone.0002297.g007

PSD-95 ablation leads to the enhanced LTP under various stimuli whereas SAP102 mutant mice show the increase under more restricted conditions [48–50]. It is proposed that these synaptic membrane-associated guanylate kinase proteins couple the NMDA receptor to distinct signaling pathways [49,51].

Functional impairment by manipulating molecules affecting plasticity or cellular signaling or both is one approach to clarifying their roles in motor control and learning [13,52–54]. While the impairment at any site of the specific neural network may affect its function, the enhancement of plasticity at a specific site would affect the network function only if the site is a rate-limiting critical site. Thus, Delphilin mutant mice should be useful for this plasticity enhancement approach because Delphilin is selectively localized at PF-PC synapses and its ablation facilitates LTD induction with little effect on the maximal amplitude of LTD expression. OKR adaptation is accompanied by a change in Purkinje neuron activities in the cerebellar flocculus [55], and LTD has been implicated in the OKR adaptation [35,56]. Since neurons are embedded in dynamic networks, some compensatory changes might occur in response to Delphilin ablation. Despite such possibility, the adaptive increase in OKR gain was significantly augmented in the Delphilin mutant mice. Thus, our results suggest the critical and rate-limiting role of LTD induction at PF-PC synapses in the neural network for OKR gain-increase adaptation, a simple form of motor learning. On the other hand, the adaptive decrease of OKR phase lag was unaltered by the mutation. In motor coordination tests, the performance of Delphilin mutant mice was also comparable to that of wild-type mice under the conditions used. Thus, the motor learning ability appears not to be generally facilitated in Delphilin mutant mice, although the possibility cannot be excluded that the conditions employed may be inadequate to detect the effect of the LTD modulation. It has been repeatedly reported that impairment of LTD is associated with motor learning deficits [13,52–54]. However, there are controversial results showing that mice with diminished LTD have normal motor learning [57,58]. Recent studies suggested that not gain-decrease vestibulo-ocular reflex (VOR) adaptation but gain-increase VOR adaptation depends on LTD and the dependence of VOR gain-increase adaptation on LTD differs depending on the frequency of training sinusoidal rotation [59,60]. It was also reported that the ablation of fragile X mental retardation protein in PCs altered spine morphology and enhanced the maximum amplitude of LTD but attenuated eyeblink conditioning [61]. Thus, it appears that the contribution of LTD in diverse forms of motor control and learning is complicated. The critical synaptic sites in cerebellar neural networks may be variable depending on the types of diverse motor control and learning. In fact, various cerebellar synapses show adaptive plasticity [2,36,62–66]. Similar complications may underlie the fact that the overexpression of NMDA receptor 2B enhances hippocampal LTP and learning [67], whereas PSD-95 mutant mice show severe impairments in spatial learning and SAP102 mutant mice have mild impairments despite of enhanced hippocampal LTP [48,49]. Further analyses will be required to clarify the issue.

The wealth of knowledge of the neural circuits makes the cerebellum an ideal system for studying the molecular and cellular mechanism of brain functions. Various cerebellar synapses show multiple forms of synaptic plasticity [2,36,62–66] and may play differential roles in diverse motor control and learning. As exemplified in this study, enhancing synaptic plasticity at a specific synaptic site of a neural network is a useful approach to understanding the roles of multiple plasticity mechanisms at various cerebellar synapses in motor control and learning.

Supporting Information

Figure S1 Anatomical analysis in the flocculus and paraflocculus. A,B, Hematoxylin staining of coronal cerebellar sections from wild-type (A) and mutant (B) mice. Co, cochlear nucleus; Fl, flocculus; PFl, paraflocculus. C–F, Double immunofluorescence for calbindin (green) and VGluT2 (red) in the flocculus (C,D) and paraflocculus (E,F) of wild-type (C,E) and mutant (D,F) mice. Asterisks indicate the cell body of PCs. ML, molecular layer. G–J, Electron micrographs of the cerebellar molecular layer of the flocculus (G,H) and paraflocculus (I,J) of wild-type (G,I) and mutant (H,J) mice. s, PC spine in contact with PF terminals. Scale bars: A, 500 μm; C, 20 μm; G, 500 nm.
Found at: doi:10.1371/journal.pone.0002297.s001 (9.87 MB TIF)

Acknowledgments

We thank R. Natsume for chimeric mouse preparation, Drs. T. Yamamoto and T. Tezuka for PTPMEG antibody, and T. Nagamoto, Y. Nakano, and T. Tsunoda for help in mice breeding. We are grateful to Dr. M. Ohtsuka for his support. Thanks are also to Drs. T. Miyazaki, S. Kakizawa, K. Hashimoto, M. Kano, K. Takehara, S. Kawahara, Y. Kirino, T. Okuno, and T. Uemura for advice.

Author Contributions

Conceived and designed the experiments: TH MM. Performed the experiments: MW TT TW GO TY MY YY MF. Analyzed the data: TT GO TY MF. Contributed reagents/materials/analysis tools: HM KS SK. Wrote the paper: MW TT TH MM GO TY MF.

References

1. Christian KM, Thompson RF (2003) Neural substrates of eyeblink conditioning: acquisition and retention. Learn Mem 10: 427–455.
2. Boyden ES, Katoh A, Raymond JL (2004) Cerebellum-dependent learning: the role of multiple plasticity mechanisms. Annu Rev Neurosci 27: 581–609.
3. Altman J, Bayer SA (1997) Development of the cerebellar system: in relation to its evolution, structure, and functions. Boca Raton: CRC Press.
4. Marr D (1969) A theory of cerebellar cortex. J Physiol 202: 437–470.
5. Albus JS (1971) A theory of cerebellar function. Math Biosci 10: 25–61.
6. Ito M (1984) The cerebellum and neural control. New York: Raven Press.
7. Yamazaki M, Araki K, Shibata A, Mishina M (1992) Molecular cloning of a cDNA encoding a novel member of the mouse glutamate receptor channel family. Biochem Biophys Res Commun 183: 886–892.
8. Araki K, Meguro H, Kushiya E, Takayama C, Inoue Y, et al. (1993) Selective expression of the glutamate receptor channel δ2 subunit in cerebellar Purkinje cells. Biochem Biophys Res Commun 197: 1267–1276.
9. Lomeli H, Sprengel R, Laurie DJ, Köhr G, Herb A, et al. (1993) The rat delta-1 and delta-2 subunits extend the excitatory amino acid receptor family. FEBS Lett 315: 318–322.
10. Takayama C, Nakagawa S, Watanabe M, Mishina M, Inoue Y (1996) Developmental changes in expression and distribution of the glutamate receptor channel δ2 subunit according to the Purkinje cell maturation. Dev Brain Res 92: 147–155.
11. Landsend AS, Amiry-Moghaddam M, Matsubara A, Bergersen L, Usami S, et al. (1997) Differential localization of δ glutamate receptors in the rat cerebellum: coexpression with AMPA receptors in parallel fiber-spine synapses and absence from climbing fiber-spine synapses. J Neurosci 17: 834–842.
12. Hirano T, Kasono K, Araki K, Mishina M (1995) Suppression of LTD in cultured Purkinje cells deficient in the glutamate receptor δ2 subunit. Neuroreport 6: 524–526.
13. Kashiwabuchi N, Ikeda K, Araki K, Hirano T, Shibuki K, et al. (1995) Impairment of motor coordination, Purkinje cell synapse formation, and cerebellar long-term depression in GluR&2 mutant mice. Cell 81: 245–252.
14. Funabiki K, Mishina M, Hirano T (1995) Retarded vestibular compensation in mutant mice deficient in δ2 glutamate receptor subunit. Neuroreport 7: 189–192.
15. Kishimoto Y, Kawahara S, Suzuki M, Mori H, Mishina M, et al. (2001) Classical eyeblink conditioning in glutamate receptor subunit δ2 mutant mice is impaired in the delay paradigm but not in the trace paradigm. Eur J Neurosci 13: 1249–1253.
16. Kurihara H, Hashimoto K, Kano M, Takayama C, Sakimura K, et al. (1997) Impaired parallel fiber->Purkinje cell synapse stabilization during cerebellar development of mutant mice lacking the glutamate receptor δ2 subunit. J Neurosci 17: 9613–9623.
17. Hashimoto K, Ichikawa R, Takechi H, Inoue Y, Aiba A, et al. (2001) Roles of glutamate receptor δ2 subunit (GluRδ2) and metabotropic glutamate receptor subtype 1 (mGluR1) in climbing fiber synapse elimination during postnatal cerebellar development. J Neurosci 21: 9701–9712.
18. Ichikawa R, Miyazaki T, Kano M, Hashikawa T, Tatsumi H, et al. (2002) Distal extension of climbing fiber territory and multiple innervation caused by aberrant wiring to adjacent spiny branchlets in cerebellar Purkinje cells lacking glutamate receptor δ2. J Neurosci 22: 8487–8503.
19. Takeuchi T, Miyazaki T, Watanabe M, Mori H, Sakimura K, et al. (2005) Control of synaptic connection by glutamate receptor δ2 in the adult cerebellum. J Neurosci 25: 2146–2156.
20. Zuo J, De Jager PL, Takahashi KA, Jiang W, Linden DJ, et al. (1997) Neurodegeneration in Lurcher mice caused by mutation in δ2 glutamate receptor gene. Nature 388: 769–773.
21. Uemura T, Kakizawa S, Yamasaki M, Sakimura K, Watanabe M, et al. (2007) Regulation of long-term depression and climbing fiber territory by glutamate receptor δ2 at parallel fiber synapses through its C-terminal domain in cerebellar Purkinje cells. J Neurosci 27: 12096–12108.
22. Miyagi Y, Yamashita T, Fukaya M, Sonoda T, Okuno T, et al. (2002) Delphilin: a novel PDZ and formin homology domain-containing protein that synaptically colocalizes and interacts with glutamate receptor δ2 subunit. J Neurosci 22: 803–814.
23. Taniguchi M, Yuasa S, Fujisawa H, Naruse I, Saga S, et al. (1997) Disruption of *semaphorin III/D* gene causes severe abnormality in peripheral nerve projection. Neuron 19: 519–530.
24. Nakamura K, Manabe T, Watanabe M, Mamiya T, Ichikawa R, et al. (2001) Enhancement of hippocampal LTP, reference memory and sensorimotor gating in mutant mice lacking a telencephalon-specific cell adhesion molecule. Eur J Neurosci 13: 179–189.
25. Fuse T, Kanai Y, Kanai-Azuma M, Suzuki M, Nakamura K, et al. (2004) Conditional activation of RhoA suppresses the epithelial to mesenchymal transition at the primitive streak during mouse gastrulation. Biochem Biophys Res Commun 318: 665–672.
26. Takahashi T, Feldmeyer D, Suzuki N, Onodera K, Cull-Candy SG, et al. (1996) Functional correlation of NMDA receptor ε subunits expression with the properties of single-channel and synaptic currents in the developing cerebellum. J Neurosci 16: 4376–4382.
27. Fukaya M, Watanabe M (2000) Improved immunohistochemical detection of postsynaptically located PSD-95/SAP90 protein family by protease section pretreatment: a study in the adult mouse brain. J Comp Neurol 426: 572–586.
28. Hironaka K, Umemori H, Tezuka T, Mishina M, Yamamoto T (2000) The protein-tyrosine phosphatase PTPMEG interacts with glutamate receptor δ2 and ε subunits. J Biol Chem 275: 16167–16173.
29. Sakimura K, Yoshida Y, Nabeshima Y, Takahashi Y (1980) Biosynthesis of the brain-specific 14-3-2 protein in a cell-free system from wheat germ extract directed with poly(A)-containing RNA from rat brain. J Neurochem 34: 687–693.
30. Fukaya M, Kato A, Lovett C, Tonegawa S, Watanabe M (2003) Retention of NMDA receptor NR2 subunits in the lumen of endoplasmic reticulum in targeted NR1 knockout mice. Proc Natl Acad Sci U S A 100: 4855–4860.
31. Nakagawa S, Watanabe M, Isobe T, Kondo H, Inoue Y (1998) Cytological compartmentalization in the staggerer cerebellum, as revealed by calbindin immunohistochemistry for Purkinje cells. J Comp Neurol 395: 112–120.
32. Miyazaki T, Fukaya M, Shimizu H, Watanabe M (2003) Subtype switching of vesicular glutamate transporters at parallel fibre-Purkinje cell synapses in developing mouse cerebellum. Eur J Neurosci 17: 2563–2572.
33. Shimuta M, Yoshikawa M, Fukaya M, Watanabe M, Takeshima H, et al. (2001) Postsynaptic modulation of AMPA receptor-mediated synaptic responses and LTP by the type 3 ryanodine receptor. Mol Cell Neurosci 17: 921–930.
34. Iwashita M, Kanai R, Funabiki K, Matsuda K, Hirano T (2001) Dynamic properties, interactions and adaptive modifications of vestibulo-ocular reflex and optokinetic response in mice. Neurosci Res 39: 299–311.
35. Katoh A, Yoshida T, Himeshima Y, Mishina M, Hirano T (2005) Defective control and adaptation of reflex eye movements in mutant mice deficient in either the glutamate receptor δ2 subunit or Purkinje cells. Eur J Neurosci 21: 1315–1326.
36. Hansel C, Linden DJ, D'Angelo E (2001) Beyond parallel fiber LTD: the diversity of synaptic and non-synaptic plasticity in the cerebellum. Nature Neurosci 4: 467–475.
37. Ito M (2002) The molecular organization of cerebellar long-term depression. Nature Rev Neurosci 3: 896–902.
38. Kim SJ, Kim YS, Yuan JP, Petralia RS, Worley PF, et al. (2003) Activation of the TRPC1 cation channel by metabotropic glutamate receptor mGluR1. Nature 426: 285–291.
39. Hirano T, Kasono K, Araki K, Shinozuka K, Mishina M (1994) Involvement of the glutamate receptor δ2 subunit in the long-term depression of glutamate responsiveness in cultured rat Purkinje cells. Neurosci Lett 182: 172–176.
40. Cesa R, Morando L, Strata P (2003) Glutamate receptor δ2 subunit in activity-dependent heterologous synaptic competition. J Neurosci 23: 2363–2370.
41. Mishina M (2003) Timing determines the neural substrates for eyeblink conditioning. Int Congr Ser 1250: 473–486.
42. Yawata S, Tsuchida H, Kengaku M, Hirano T (2006) Membrane-proximal region of glutamate receptor δ2 subunit is critical for long-term depression and interaction with protein interacting with C kinase 1 in a cerebellar Purkinje neuron. J Neurosci 26: 3626–3633.
43. Yasumura M, Uemura T, Yamasaki M, Sakimura K, Watanabe M, et al. (2008) Role of the internal Shank-binding segment of glutamate receptor δ2 in synaptic localization and cerebellar functions. Neurosci Lett 433: 146–151.
44. Roche KW, Ly CD, Petralia RS, Wang YX, McGee AW, et al. (1999) Postsynaptic density-93 interacts with the δ2 glutamate receptor subunit at parallel fiber synapses. J Neurosci 19: 3926–3934.
45. Yue Z, Horton A, Bravin M, DeJager PL, Selimi F, et al. (2002) A novel protein complex linking the δ2 glutamate receptor and autophagy: implications for neurodegeneration in lurcher mice. Neuron 35: 921–933.
46. Yap CC, Muto Y, Kishida H, Hashikawa T, Yano R (2003) PKC regulates the δ2 glutamate receptor interaction with S-SCAM/MAGI-2 protein. Biochem Biophys Res Commun 301: 1122–1128.
47. Kina S, Tezuka T, Kusakawa S, Kishimoto Y, Kakizawa S, et al. (2007) Involvement of protein-tyrosine phosphatase PTPMEG in motor learning and cerebellar long-term depression. Eur J Neurosci 26: 2269–2278.
48. Migaud M, Charlesworth P, Dempster M, Webster LC, Watabe AM, et al. (1998) Enhanced long-term potentiation and impaired learning in mice with mutant postsynaptic density-95 protein. Nature 396: 433–439.
49. Cuthbert PC, Stanford LE, Coba MP, Ainge JA, Fink AE, et al. (2007) Synapse-associated protein 102/dlgh3 couples the NMDA receptor to specific plasticity pathways and learning strategies. J Neurosci 27: 2673–2682.
50. Komiyama NH, Watabe AM, Carlisle HJ, Porter K, Charlesworth P, et al. (2002) SynGAP regulates ERK/MAPK signaling, synaptic plasticity, and learning in the complex with postsynaptic density 95 and NMDA receptor. J Neurosci 22: 9721–9732.
51. Kim MJ, Dunah AW, Wang YT, Sheng M (2005) Differential roles of NR2A- and NR2B-containing NMDA receptors in Ras-ERK signaling and AMPA receptor trafficking. Neuron 46: 745–760.
52. De Zeeuw CI, Hansel C, Bian F, Koekkoek SKE, van Alphen AM, et al. (1998) Expression of a protein kinase C inhibitor in Purkinje cells blocks cerebellar LTD and adaptation of the vestibulo-ocular reflex. Neuron 20: 495–508.
53. Feil R, Hartmann J, Luo C, Wolfsgruber W, Schilling K, et al. (2003) Impairment of LTD and cerebellar learning by Purkinje cell-specific ablation of cGMP-dependent protein kinase I. J Cell Biol 163: 295–302.

54. Koekkoek SKE, Hulscher HC, Dortland BR, Hensbroek RA, Elgersma Y, et al. (2003) Cerebellar LTD and learning-dependent timing of conditioned eyelid responses. Science 301: 1736–1739.
55. Nagao S (1988) Behavior of floccular Purkinje cells correlated with adaptation of horizontal optokinetic eye movement response in pigmented rabbits. Exp Brain Res 73: 489–497.
56. Katoh A, Kitazawa H, Itohara S, Nagao S (2000) Inhibition of nitric oxide synthesis and gene knockout of neuronal nitric oxide synthase impaired adaptation of mouse optokinetic response eye movements. Learn Mem 7: 220–226.
57. Welsh JP, Yamaguchi H, Zeng XH, Kojo M, Nakada Y, et al. (2005) Normal motor learning during pharmacological prevention of Purkinje cell long-term depression. Proc Natl Acad Sci U S A 102: 17166–17171.
58. Faulstich M, van Alphen AM, Luo C, du Lac S, De Zeeuw CI (2006) Oculomotor plasticity during vestibular compensation does not depend on cerebellar LTD. J Neurophysiol 96: 1187–1195.
59. Boyden ES, Katoh A, Pyle JL, Chatila TA, Tsien RW, et al. (2006) Selective engagement of plasticity mechanisms for motor memory storage. Neuron 51: 823–834.
60. Hansel C, de Jeu M, Belmeguenai A, Houtman SH, Buitendijk GHS, et al. (2006) αCaMKII is essential for cerebellar LTD and motor learning. Neuron 51: 835–843.
61. Koekkoek SKE, Yamaguchi K, Milojkovic BA, Dortland BR, Ruigrok TJH, et al. (2005) Deletion of *FMR1* in Purkinje cells enhances parallel fiber LTD, enlarges spines, and attenuates cerebellar eyelid conditioning in Fragile X syndrome. Neuron 47: 339–352.
62. Ito M (1982) Cerebellar control of the vestibulo-ocular reflex–around the flocculus hypothesis. Annu Rev Neurosci 5: 275–297.
63. Jörntell H, Hansel C (2006) Synaptic memories upside down: bidirectional plasticity at cerebellar parallel fiber-Purkinje cell synapses. Neuron 52: 227–238.
64. Liu SJ, Cull-Candy SG (2000) Synaptic activity at calcium-permeable AMPA receptors induces a switch in receptor subtype. Nature 405: 454–458.
65. Pugh JR, Raman IM (2006) Potentiation of mossy fiber EPSCs in the cerebellar nuclei by NMDA receptor activation followed by postinhibitory rebound current. Neuron 51: 113–123.
66. Zhang W, Linden DJ (2006) Long-term depression at the mossy fiber-deep cerebellar nucleus synapse. J Neurosci 26: 6935–6944.
67. Tang YP, Shimizu E, Dube GR, Rampon C, Kerchner GA, et al. (1999) Genetic enhancement of learning and memory in mice. Nature 401: 63–69.

Neurology Asia 2008; 13 : 203 – 204

Anti-aquaporin 4 antibody test in a large series of Japanese optic-spinal multiple sclerosis and neuromyelitis optica

[1]K Tanaka, [2]T Tani, [3]M Tanaka, [4]M Nishizawa, [4]K Sakimura, [1]M Matsui

[1]Kanazawa Medical University, Ishikawa; [2]Nishi-Niigata Chuo National Hospital; [3]Utano National Hosp, Kyoto; [4]Brain Research Institute, Niigata University, Niigata, Japan

Anti-aquaporin 4 antibody (AQP4-Ab) is detected specifically with high sensitivity in optic-spinal form of multiple sclerosis (OSMS)/neuromyelitis optica (NMO). We established the immunofluorescence detection system of NMO-IgG and AQP4 antibody (AQP4-Ab) using human AQP4 cDNA-transfected HEK 293 cells and examined NMO-IgG/AQP4-Ab in a large series of Japanese OSMS/NMO patients since 2006.

As for NMO-IgG detection, we used cryostat sections from rat cerebrum and cerebellum with indirect immunofluorescence detection system. For AQP4-Ab detection, we cloned human AQP4-cDNA from human brain total RNA. The cDNA was then inserted into expression vector, and HEK 293 cells were transfected with this vector. The cells were then fixed with 4% paraformaldehyde/PBS, incubated with the patients' sear or CSF, and finally with FITC-conjugated anti-human IgG.

We tested AQP4-Ab in 2,076 samples with Japanese OSMS/NMO patients and found 569 AQP4-Ab positive cases. Among them, 450 of AQP4-Ab positive sera/CSF were from women (79.1%). AQP4-Ab positive group showed higher age of onset, higher percentages of blind or bed-ridden patients, higher EDSS scores; 75% of them showed long spinal cord lesions of more than three vertebrate segments on spinal MRI (Table 1).

Those with AQP4-Ab negative contained heterogeneous group of patients, so we compared the clinical features between AQP4-Ab positive or negative group among those with long spinal cord lesions.

Higher percentage of AQP-Ab positive patients with long spinal cord lesions were associated with Sjögren syndrome and frequently detected autoantibodies such as ANA or SS-A and SS-B. Our study with large series confirmed the characteristic features of AQP4-Ab positive group with strong

Table 1: Clinical features in AQP4-Ab (+) optic-spinal multiple sclerosis/neuromyelitis optica patients

Study parameter	AQP4-Ab (+)
Number (men/women)	569 (119/450) (women: 79.1%)
Age at onset in years	47.2±16.3
Relapsing remitting/secondary progressive/primary progressive in percent	75.8/8.1/1.3
EDSS score	6.2±2.1
Wheel chair bound/bed ridden	85/138 (38.1%)
Severe visual loss (blind)	99/116 (46.0%)
First lesion (Optic nerve/spinal cord/brainstem/cerebrum) in percent	43.9/41.0/8.1/7.0
MRI (cerebrum/cerebellum/brainstem) in percent	35.9/4.8/22.3
MRI long cord lesion (+/–) in percent	74.1/7.6
Oligoclonal band (+)/MBP (+) in percent	10.4/57.4

co-relations to female preponderance, higher age at onset, long spinal cord lesions, severe optic and spinal symptoms and other autoimmune diseases.

However, certain amount of overlap was seen between AQP4-Ab positive and negative patients. It is not yet clear that AQP4-Ab is the essential pathognomonic factor or diagnostic marker, but the certain clinical features seen in the AQP4-Ab positive cases are clearly differed from classic MS. Those with AQP4-Ab negative group might be heterogeneous with those having low titer AQP4-Ab which could not be detected by the present assay system.

To clarify the significance of AQP4-Ab, we need to show the direct role of AQP4-Ab for NMO.

References

1. Tanaka K, Tani T, Tanaka M, *et al*. Anti-aquaporin 4 antibody in Japanese multiple sclerosis with long spinal cord lesions. *Mult Scler* 2007; 13: 850-5.
2. Tanaka M, Tanaka K, Komori M, Saida T. Anti-aquaporin 4 antibody in Japanese multiple sclerosis: the presence of optic spinal multiple sclerosis without long spinal cord lesions and anti-aquaporin 4 antibody. *J Neurol Neurosurg Psychiatry* 2007; 78: 990-2.

ELSEVIER

Journal of Neuroimmunology 196 (2008) 166–169

Journal of
Neuroimmunology

www.elsevier.com/locate/jneuroim

Short communication

Regulatory T cells in paraneoplastic neurological syndromes

Takashi Tani [a], Keiko Tanaka [a,*], Jiro Idezuka [b], Masatoyo Nishizawa [a]

[a] *Neurology, Brain Research Institute of Niigata University, Asahimachi Dori 1-757, Nitgata-shi, Niigata, Japan*
[b] *Ojiya Sakura hospital, Kowada 2732, Ojiya-shi, Niigata, Japan*

Received 29 January 2008; received in revised form 4 March 2008; accepted 6 March 2008

Abstract

Focusing on $CD4^+CD25^+$ regulatory T lymphocytes (T_{reg}), we studied the gene expression of T_{reg} functional molecules in peripheral blood lymphocytes of patients with paraneoplastic neurological syndrome (PNS), including Lambert–Eaton myasthenic syndrome (LEMS) with small cell lung carcinoma (SCLC) and anti-Hu- or anti-Yo-antibody-positive PNS. T_{reg}-rich subsets were sorted from the patients' peripheral blood mononuclear cells, and the mRNA expression levels of their functional genes were measured. The expression levels of FOXP3, TGF-β and CTLA4 mRNA in T_{reg}-rich subsets of PNS patients were down-regulated compared with that of SCLC patients without PNS. These results suggest that T_{reg} dysfunction plays a role in PNS development.

Keywords: Paraneoplastic neurological syndrome; CD4+CD25+ regulatory T cell; FOXP3

1. Introduction

Paraneoplastic neurological syndromes (PNS) are thought to be a result of immunological mechanisms, in that, the mechanisms of cancer immunity and autoimmunity in neuronal tissues are both elicited in PNS. Because tumors are often too small to be detected with a conventional screening system, antitumor immunity might be accelerated at least in the early stage of PNS. Furthermore, PNS develops in a small population of patients with similar tumor pathologies, suggesting that PNS patients have special immunological backgrounds for tuning up immunity to tumors and autoimmunity in nervous tissues. However, these backgrounds have not been analyzed extensively in PNS. Therefore, we studied the immunological background of PNS. We focused on the immunoregulatory system, since regulatory system dysfunction might lead to the deterioration of immunotolerance that accelerates both autoimmunity and antitumor immunological reactions.

In the immunoregulatory system, $CD4^+CD25^+$ regulatory T cells (T_{reg}) play important roles. Their master gene is the *forkhead/winged-helix family transcription factor gene Foxp3* (Brunkow et al., 2001; Khattri et al., 2001; Fontenot et al., 2003), whereas the target gene of immune dysregulation polyendocrinopathy, enteropathy, X-linked syndrome (IPEX) is the human ortholog *FOXP3*. T_{reg} suppresses immunoreaction, and its dysfunction causes immunotolerance breakdown and organ-specific autoimmune diseases. Cytotoxic-T-lymphocyte-associated antigen 4 (CTLA-4) on T_{reg} interacts with members of the B7 family on antigen-presenting cells and suppresses effector T lymphocyte functions in different ways (Wing et al., 2006; Sansom and Walker, 2006). Effector T cell activation is inhibited by transforming growth factor-β (TGF-β) induced by CTLA-4. The glucocorticoid-induced tumor-necrosis factor receptor family-related molecule (GITR) is also an important functional molecule in T_{reg} (Esparza and Arch, 2006).

In this study, we analyzed the mRNA expression of T_{reg} functional molecules in a T_{reg}-rich subset in the peripheral blood of PNS patients to determine whether the immunoregulatory system is compromised in PNS, and found that the expressions of FOXP3, TGF-β and CTLA-4 mRNAs are suppressed in PNS patients compared with those in cancer patients without PNS.

2. Materials and methods

2.1. Patients

We analyzed peripheral blood samples from three anti-Hu-antibody-positive PNS patients (Hu group; a man with striatal encephalitis, a man with ataxic sensory neuropathy and a

* Corresponding author. Tel.: +81 25 227 0666; fax: +81 25 223 6646.
E-mail address: nrg45889@nifty.com (K. Tanaka).

0165-5728/$ - see front matter © 2008 Elsevier B.V. All rights reserved.
doi:10.1016/j.jneuroim.2008.03.002

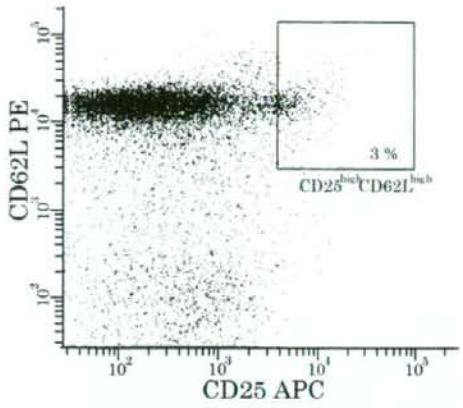

Fig. 1. A T_{reg}-rich subset is shown in the cytogram (*X*-axis, CD25; *Y*-axis, CD62L; gated on lymphocytes and CD4-positive). To decline the contamination of CD4-positive T cells having different character, highest 3% of total CD4-positive lymphocytes were sorted.

woman with ataxic sensory neuropathy with SCLC; mean age, 63±7, their sera or CSF were examined by western blot using recombinant Hu antigen proteins and revealed to be positive for the anti-Hu-antibody), two anti-Yo-antibody-positive PNS patients (Yo group; an 81-year-old woman with subacutely-evolved cerebellar ataxia and breast carcinoma and a 50-year-old woman with progressive cerebellar ataxia being bed-ridden within two weeks and found ovarian cancer six months later, their sera and CSF were examined by western blot using recombinant Yo antigen proteins and revealed to be positive for anti-Yo-antibody), and five Lambert–Eaton myasthenic syndrome (LEMS) patients (the diagnosis were made by their clinical and electrodiagnostic features and the presence of the anti-voltage-gated-calcium-channel (VGCC) antibody) with SCLC (three men and two women; mean age 68±13) (LEMS group). As for controls, four SCLC patients without neurological diseases (PNS (−) SCLC group; two men and two women; mean age, 67±9, negative for anti-Hu/Yo/VGCC antibodies) and four healthy people (HC group; two men and two women; mean age, 38±9, without anti-Hu/Yo/VGCC antibodies) were also examined.

The diagnosis of SCLC was confirmed cytologically or histologically in each patient. All of them were in the limited stage without remote metastasis. All of the samples tested were obtained before anti-cancer therapy or immunomodulation therapy.

2.2. Monoclonal antibodies

The monoclonal antibodies fluorescein isothiocyanate (FITC)-conjugated anti-human CD4 (Sigma-Aldrich, Inc.), allophycocyanin (APC)-conjugated anti-CD25, and phycoerythrin (PE)-conjugated anti-CD62L (BD Biosciences Pharmingen) antibodies were used. The concentrations of these antibodies were in accordance with the manufacturer's instructions when labeling the PBMC samples.

2.3. Cell sorting

Peripheral blood mononuclear cells (PBMCs) were obtained from heparinized venous blood by the Ficoll–Paque density gradient method, and FITC-anti-CD4, APC-anti-CD25 and PE-anti-CD62L antibodies were added to the PBMCs; the resulting mixture was incubated on ice for 45 min. They were then washed once with phosphate-buffered saline and analyzed on a FACS Aria cell sorter (BD Biosciences) using FACSDiva software. Approximately 10,000 $CD4^+CD25^{high}CD62L^{high}$ lymphocytes were sorted (Fig. 1).

2.4. RNA extraction and PCR analysis

Total RNA was extracted from the sorted $CD4^+CD25^{high}CD62L^{high}$ cells with an RNeasy Mini kit (QIAGEN) and reverse-transcribed using a QuantiTect Reverse Transcription kit (QIAGEN) in accordance with the manufacturer's instructions. Validated primer-probe sets and QuantiTect Probe kits used in the real-time polymerase chain reaction (PCR) for detecting FOXP3, TGF-β1 and glyceraldehyde-3-phosphate dehydrogenase (GAPDH) mRNA expressions, and validated primer sets and QuantiTect SYBR Green kits for detecting CTLA-4, GITR and GAPDH mRNA expressions were purchased from QIAGEN. Real-time PCR reactions of each gene were analyzed in triplicate with an ABI PRISM 7900 sequence detector (Applied Biosystems). cDNA concentration was calculated using a standard curve and revised with GAPDH cDNA concentration. The standard cDNA solution was prepared from 1×10^8 PBMCs as described above.

Statistical comparisons between groups were performed using the Wilcoxon rank sum test.

3. Results

We analyzed the mRNA expressions of FOXP3, TGF-β1, CTLA-4 and GITR to estimate the function of T_{reg} in T_{reg}-rich

Table 1
Comparison of mRNA expressions of Treg functional molecules between study groups

Group	Number	Sex (M/F)	Age (mean±SD)	mRNA expression			
				FOXP3	TGF-β1	CTLA-4	GITR
Healthy control	4	2/2	38±9	110.1±80.2	0.71±0.32	3.53±0.28	1.74±0.56
PNS(−) SCLC	4	2/2	67±9	193.7±102.0	0.99±0.32	5.55±1.61	2.67±0.65
LEMS	5	3/2	68±13	52.5±42.1*	0.66±0.37	1.83±1.70*	1.99±1.49
Hu/Yo	5	2/3	64±12	44.0±28.5*	0.45±0.09*	2.25±2.46	1.68±1.15

* $p<0.05$ compare with PNS(−) SCLC group.

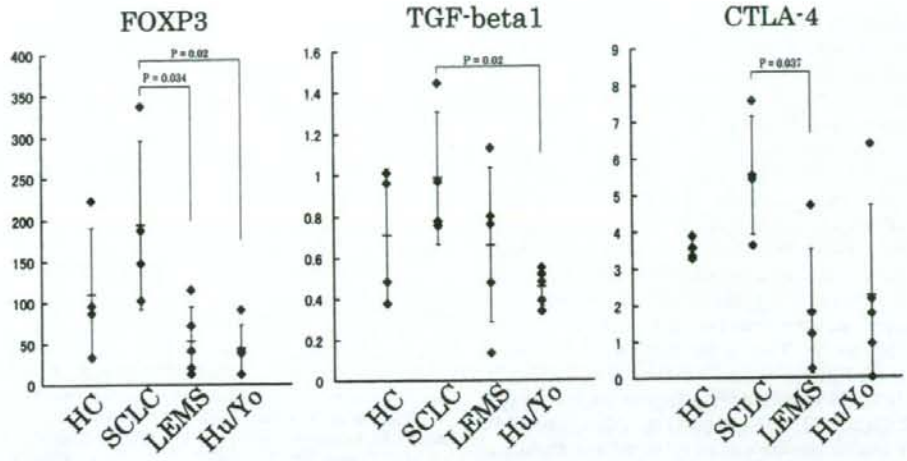

Fig. 2. Relative expressions of functional genes in T_{reg}-rich subsets of peripheral blood lymphocytes. The graphs show the mRNA relative expression ratios of the described genes (*FOXP3*, *TGF-β1* and *CTLA-4*) compared with the mRNA expression ratio of total PBMCs. LEMS; patients with Lambert–Eaton myasthenic syndrome, Hu/Yo; patients with anti-Hu- or anti-Yo-antibody-positive PNS, SCLC; SCLC patients without neurological symptoms, HC; healthy controls.

$CD4^+CD25^{high}CD62L^{high}$ subsets. The relative expression ratios compared with that of a standard cDNA solution are shown (Table 1, Fig. 2). The FOXP3 expression level of the LEMS group was less than that of the PNS (−) SCLC group (mean ± SD 52.5 ± 42.1 vs 193.7 ± 102; $P = 0.034$); that of the Hu/Yo group was also less than that of the PNS (−) SCLC group (44.0 ± 28.5 vs 193.7 ± 102.0; $P = 0.02$). The TGF-β1 expression level of the Hu/Yo group was less than that of the PNS (−) SCLC group (0.45 ± 0.09 vs 0.99 ± 0.32; $P = 0.02$). The CTLA-4 expression level of the LEMS group was less than that of the PNS (−) SCLC group (1.83 ± 1.70 vs 5.55 ± 1.61; $P = 0.037$). The GITR expression level of the four groups did not significantly differ.

4. Discussion

For the pathogenesis of PNS, it is speculated that an antigen expressed on a tumor elicits immunity against tumors which cross reacts with certain neuronal tissues and causes autoimmune reactions in nervous tissues. However, PNS develops in very few patients suggesting that some predisposing factors exist in PNS patients. In this study, we hypothesized that immunoregulatory system dysfunction causes a dysregulated immunological reaction to tumors and nervous tissues in PNS patients. To test this hypothesis, we examined the FOXP3, TGF-β1 and CTLA-4 mRNA expression, the functional molecules in T_{reg}-rich subsets in PBMCs from PNS patients, and found that the expression is predominantly depressed in the LEMS and Hu/Yo groups.

The LEMS and Hu/Yo groups were each divided into separate groups, because LEMS is thought to be an antibody-mediated disease, since VGCC-antibody-containing patient serum IgG could block an excitation-transmission coupling at the neuromuscular junction (Lang et al., 1981), whereas anti-Hu or anti-Yo-positive PNS is thought to be a cytotoxic-T-cell-mediated disease, since oligoclonal cytotoxic T cells are located around the lesions and can recognize and kill neurons (Albert et al., 1998; Tanaka et al., 1999; Neumann et al., 2002; Dalmau and Bataller, 2006). There has not been established an animal model to prove the pathomechanisms via T cell-mediated autoimmunity in the PNS with anti-Yo or anti-Hu antibody, however, these antibodies could not elicite the neuronal damage suggested having different mechanisms with those antibody-mediated PNS like LEMS.

We used CD62L as a T_{reg} surface marker, because $CD4^+CD25^+CD62L^{high}$ population had important roles in immunoregulation, shown in an examination about developing diabetes in non-obase-diabetic(NOD) mouse, which is a model for type 1 diabetes. Natural $CD4^+CD25^+$ T_{reg} cells have been defined based on a $CD62L^{high}$ surface phenotype and expression of markers, such as CTLA-4, GITR. $CD4^+CD62L^{high}$ T cells that were prepared from the thymus or spleen of young NOD mice block diabetes in adoptive transfer experiments (Szanya et al., 2002; Shannon et al., 2005). Naïve T cells that gained the regulatory functional master gene *Foxp3* are considered to have a naturally occurring T_{reg} phenotype and express CTLA-4, GITR and CD103 (Hori et al., 2003). Thus, *Foxp3* expression affects the expressions of the genes encoding these functional molecules.

We compared the FOXP3 expression using flow cytometer that showed higher in $CD62L^{high}$ group than $CD62L^{low}$ (data not shown), so $CD62L^{high}$ population was selected for the quantitation of mRNA expression of functional molecules which we thought more specific population for T_{reg} function.

A decrease in the T_{reg} population and an alteration in the T_{reg} function have been reported in other organ-specific autoimmune diseases (Viglietta et al., 2004; Crispin et al., 2003; Liu et al., 2004; Takahashi et al., 2006). Thus, the T_{reg} function is often suppressed and the population frequency is often reduced in

autoimmune diseases. T_{reg} is expected to apply in autoimmune disease therapy because tissue-specific T_{reg} suppresses autoreactive T cells and can prevent autoimmune diseases (Fisson et al., 2006). Conversely, in cancer patients, the T_{reg} population tends to increase in peripheral blood, ascites, pleural effusion and lesion tissues (Yang et al., 2006; Cesana et al., 2006; Baecher-Allan and Anderson, 2006). The T_{reg} population increase in and around cancer tissues might be followed by the down-regulation of antitumor immunity, thereby contributing to cancer growth (Jarnicki et al., 2006). Our data showing upregulation of some of the T_{reg}-related molecules in those with SCLC without PNS might be relevant to this hypothesis. However, there have been no reports on a regulatory system evaluations in PNS so far. This is the first report showing a dysfunction in the immunoregulatory system in PNS.

In this analysis, we divided the PNS patients into two groups, namely, the LEMS and Hu/Yo groups. Anti-VGCC antibodies in the LEMS patients are thought to cause the functional impairment of the transmission of neuromuscular junctions whereas the sera containing anti-Yo or anti-Hu antibody from the PNS patients could not elicit the neuronal damage suggested having different mechanisms with those antibody-mediated PNS as LEMS. Thus, the pathogeneses of the disorders in both groups might be different, but both disorders also share the similar features: a hyperimmune state producing antibodies or T cells that attack certain nervous tissues. As we showed in this study, T_{reg} functional gene expression level was reduced in both groups, supporting our hypothesis of an immunoregulatory system dysfunction in PNS.

In summary, to clarify the pathogenesis of PNS at the point of immunoregulatory system abnormalities, we analyzed the functional gene expression of T_{reg}-rich subsets, and found low gene expression level of these molecules in PNS patients.

References

Albert, M., Darnell, J.C., Bender, A., Francisco, L.M., Bhardwaj, N., Darnell, R.B., 1998. Tumor-specific killer cells in paraneoplastic cerebellar degeneration. Nat. Med. 11, 1321–1324.

Baecher-Allan, C., Anderson, D.E., 2006. Immune regulation in tumor-bearing hosts. Curr. Opin. Immunol. 18, 214–219.

Brunkow, M.E., Jeffery, E.W., Hjerrild, K.A., Paeper, B., Clark, L.B., Yasayko, S.-A., Wilkinson, J.E., Galas, D., Ziegler, S.F., Ramsdell, F., 2001. Disruption of a new forkhead/winged-helix protein, scurfin, results in the fatal lymphoproliferative disorder of the scurfy mouse. Nat. Genet. 27, 68–73.

Cesana, G.C., DeRaffele, G., Cohen, S., Moroziewicz, D., Mitcham, J., Stoutenburg, J., Cheung, K., Hesdorffer, C., Kim-Schulze, S., Kaufman, H.L., 2006. Characterization of $CD4^+CD25^+$ regulatory T cells in patients treated with high-dose interleukin-2 for metastatic melanoma or renal cell carcinoma. J. Clin. Oncol. 24, 1169–1177.

Crispin, J.C., Martínez, A., Alcocer-Varela, J., 2003. Quantification of regulatory T cells in patients with systemic lupus erythematosus. J. Autoimmun. 21, 273–276.

Dalmau, J., Bataller, L., 2006. Clinical and immunological diversity of limbic encephalitis: a model for paraneoplastic neurologic disorders. Hematol. Oncol. Clin. North. Am. 20, 1319–1335.

Esparza, E.M., Arch, R.H., 2006. Signaling triggered by glucocorticoid-induced tumor necrosis factor receptor family-related gene: regulation at the interface between regulatory T cells and immune effector cells. Front. Biosci. 11, 1448–1465.

Fisson, S., Djelti, F., Trenado, A., Billiard, F., Liblau, R., Klatzmann, D., Cohen, J.L., Salomon, B.L., 2006. Therapeutic potential of self-antigen-specific CD4+CD25+ regulatory T cells selected in vitro from a polyclonal repertoire. Eur. J. Immunol. 36, 817–827.

Fontenot, J.D., Gavin, M.A., Rudensky, A.Y., 2003. Foxp3 programs the development and function of CD4+CD25+ regulatory T cells. Nat. Immunol. 4, 330–336.

Hori, S., Nomura, T., Sakaguchi, S., 2003. Control of regulatory T cell development by the transcription factor *Foxp3*. Science 299, 1057–1061.

Jarnicki, A.G., Lysaght, J., Todryk, S., Mills, K.H.G., 2006. Suppression of antitumor immunity by IL-10 and TGF-β-producing T cells infiltrating the growing tumor: influence of tumor environment on the induction of $CD4^+$ and $CD8^+$ regulatory T cells. J. Immunol. 177, 896–904.

Khattri, R., Kasprowicz, D., Cox, T., Mortrud, M., Appleby, M.W., Brunkow, M.E., Ziegler, S.F., Ramsdell, F., 2001. The amount of scurfin protein determines peripheral T cell number and responsiveness. J. Immunol. 167, 6312–6320.

Lang, B., Newsom-Davis, J., Wray, D., Vincent, A., Murray, N., 1981. Autoimmune aetiology for myasthenic (Eaton–Lambert) syndrome. Lancet 2 (8240), 224–226.

Liu, M.F., Wang, C.R., Fung, L.L., Wu, C.R., 2004. Decreased CD4+CD25+ T cells in peripheral blood of patients with systemic lupus erythematosus. Scand. J. Immunol. 59, 198–202.

Neumann, H., Medana, I.S., Baier, J., Lassmann, H., 2002. Cytotoxic T lymphocytes in autoimmune and degenerative CNS diseases. Trends. Neurosci. 25, 313–319.

Sansom, D.M., Walker, L.S.K., 2006. The role of CD28 and cytotoxic T-lymphocyte antigen-4 (CTLA-4) in regulatory T-cell biology. Immunol. Rev. 212, 131–148.

Shannon, M.P., Carmen, P.W., Donna, A.C., Stephen, H.C., Roland, T., 2005. Single cell analysis shows decreasing FoxP3 and TGFβ1 coexpressing $CD4^+CD25^+$ regulatory T cells during autoimmune diabetes. J. Exp. Med. 201, 1333–1346.

Szanya, V., Ermann, J., Taylor, C., Holness, C., Fathman, C.G., 2002. The subpopulation of CD4+CD25+ splenocytes that delays adoptive transfer of diabetes expresses L-selectin and high levels of CCR7. J. Immunol. 169, 2461–2465.

Takahashi, M., Nakamura, K., Honda, K., Kitamura, Y., Mizutani, T., Araki, Y., Kabemura, T., Chijiiwa, Y., Harada, N., Nawata, H., 2006. An inverse correlation of human peripheral blood regulatory T cell frequency with the disease activity of ulcerative colitis. Dig. Dis. Sci. 51, 677–686.

Tanaka, K., Tanaka, M., Inuzuka, T., Nakano, R., Tsuji, S., 1999. Cytotoxic T lymphocyte-mediated cell death in paraneoplastic sensory neuronopathy with anti-Hu antibody. J. Neurol. Sci. 163, 159–162.

Viglietta, V., Baecher-Allan, C., Weiner, H.L., Hafler, D.A., 2004. Loss of functional suppression by $CD4^+CD25^+$ regulatory T cells in patients with multiple sclerosis. J. Exp. Med. 199, 971–979.

Wing, K., Fehérvári, Z., Sakaguchi, S., 2006. Emerging possibilities in the development and function of regulatory T cells. Int. Immunol. 18, 991–1000.

Yang, X.H., Yamagiwa, S., Ichida, T., Matsuda, Y., Sugahara, S., Watanabe, H., Sato, Y., Abo, T., Horwitz, D.A., Aoyagi, Y., 2006. Increase of CD4DCD25D regulatory T-cells in the liver of patients with hepatocellular carcinoma. J. Hepatol. 45, 254–262.

European Journal of Neurology 2008, 15: 1075–1079 doi:10.1111/j.1468-1331.2008.02249.x

Epidemiological study of acute encephalitis in Tottori Prefecture, Japan

K. Wada-Isoe[a], M. Kusumi[a,b], T. Kai[b], E. Awaki[c], M. Shimoda[d], H. Yano[e], K. Suzuki[f], H. Nakayasu[f], K. Oota[g], H. Kowa[a] and K. Nakashima[a]

[a]*Department of Neurology, Faculty of Medicine, Institute of Neurological Sciences, Tottori University;* [b]*Department of Neurology, San-in Rosai Hospital, Yonago;* [c]*Department of Neurology, Saiseikai Sakaiminato General Hospital, Sakaiminato, Japan;* [d]*Department of Neurology, Nojima Hospital, Kurayoshi, Japan;* [e]*Department of Neurology, Tottori Municipal Hospital;* [f]*Department of Neurology, Tottori Prefectural Central Hospital; and* [g]*Department of Neurology, Tottori Red Cross Hospital, Tottori, Japan*

Keywords:
acute encephalitis, epidemiology, herpes simplex, incidence, limbic encephalitis

Received 30 April 2008
Accepted 6 June 2008

Background and purpose: To conduct an epidemiological survey of acute encephalitis focusing on non-herpetic acute limbic encephalitis (NHALE) in Tottori Prefecture, western area of Japan. *Methods:* A questionnaire survey on the annual number of patients aged 16 years or more with acute encephalitis from 2001 to 2005 was undertaken in 2006. *Results:* During the study period, 49 patients were diagnosed with acute encephalitis. The subtype of acute encephalitis was as follows: 10 patients with herpes simplex encephalitis (HSE), 12 patients with NHALE, 4 patients with paraneoplastic encephalitis, 2 patients with encephalitis associated with collagen disease, one patient with viral encephalitis other than HSE, 20 patients with encephalitis with unknown causes. The service-based incidence rate of acute encephalitis was 19.0 per million person-years. The incidence rate of NHALE subtype was 4.7 per million person-years. *Conclusions:* Our epidemiological survey indicated an estimated 550 patients would develop NHALE per year in Japan, suggesting that NHALE may not be a rare disorder.

Introduction

Few epidemiological surveys have been conducted concerning acute encephalitis in Japan [1–3]. The nationwide epidemiological survey of encephalitis conducted by Kamei and Takasu [3] indicated an annual prevalence of encephalitis to be 17.7 per million population. Recent Japanese surveys identified non-herpetic acute limbic encephalitis (NHALE) as a new subgroup of limbic encephalitis with the spectrum that excludes herpes simplex encephalitis (HSE) and paraneoplastic limbic encephalitis [4,5]. However, none of the previous epidemiological studies paid attention to NHALE and the incidence rate of this disorder remains unclear. Here, we report a questionnaire survey of acute encephalitis focusing on NHALE undertaken in Tottori Prefecture in Japan.

Materials and methods

We performed a retrospective surveillance of patients with acute encephalitis in Tottori Prefecture using a questionnaire survey. Tottori Prefecture is located in a rural area of western Japan (Fig. 1); it had a population of 607271 (290059 men and 317212 women) in 2005.

In 2006, we sent inquiries with registration criteria for each category of acute encephalitis to the departments of neurology of the 11 hospitals in Tottori Prefecture that accept patients with neurological emergencies. We asked if they had admitted any patient with acute encephalitis in an adult (≥16 years of age) patient during the 5 years from 2001 to 2005. The questionnaire enquired about type of acute encephalitis, sex and age of patient and presentation on day of onset.

The acute encephalitis group included patients with combined abnormal cerebrospinal fluid (CSF), EEG and/or neuroimaging (CT or MRI) findings with clinical signs and symptoms of acute (≤4 weeks duration) CNS involvement, that is, lowered level of consciousness, altered personality, epileptic seizures or focal neurological signs in the absence of evidence of vascular, malignant, metabolic, psychiatric, demyelinating, toxic or traumatic aetiology. Defined microbiological tests included PCR tests on CSF samples and antibody analysis of serum and CSF for herpes simplex virus and other viruses. Diagnosis of NHALE in these patients with acute encephalitis was made according to the flow chart shown in Fig. 2. Briefly, NHALE was diagnosed in patients who showed the presence of MRI abnormalities in the limbic system and/or the presence of clinical symptoms and signs that indicated

Correspondence: Kenji Wada-Isoe, Department of Neurology, Faculty of Medicine, Institute of Neurological Science, Tottori University, 36-1 Nishi-cho, Yonago, 683-8504, Japan (tel.: +81 859 38 6757; fax: +81 859 38 6759; e-mail: kewada@med.tottori-u.ac.jp).

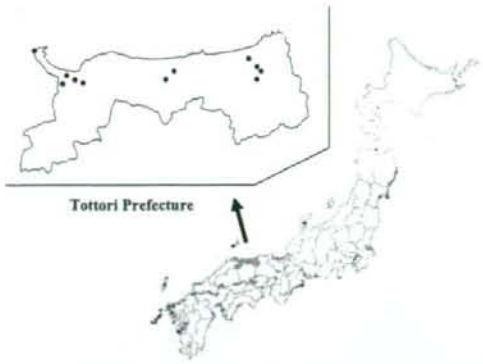

Figure 1 Location of the surveyed hospitals in Tottori Prefecture. Tottori Prefecture is located in western Japan. The eleven marked hospitals (circles) were included in our survey.

abnormalities of the limbic system, and who did not have any proven viral infection, cancer or autoimmune disorders such as systemic lupus erythematosus and autoimmune connective tissue disorders. We excluded patients with CNS infections of bacterial (including tuberculosis) and fungal origin from analysis. All patients were assessed by at least one Japanese Neurological Society board-certified neurologist and all information collected in our survey was based on official records from each patient.

The recovery rate of questionnaires was 11 of 11 departments (100%). Responses from all departments were reviewed at the Department of Neurology, Tottori University. Incidence rates per million person-years of acute encephalitis were calculated using the actual number of patients listed in the returned questionnaires. This study was planned and conducted in accordance with the Declaration of Helsinki. The Ethics Committee of Tottori University Faculty of Medicine approved the study prior to its implementation.

Results

Incidence of acute encephalitis

A total of 49 patients (30 male patients, 19 female patients) with acute encephalitis were reported during the 5 years (Table 1). Based on these results, the incidence rate of acute encephalitis was calculated to be 19.0 per million person-years (95% CI = 14.4–25.1). The number and the incidence rate were highest among men in their seventies, whilst for women the incidence was highest among women in their twenties.

Subtypes of acute encephalitis

The subtypes of the 49 patients with acute encephalitis are shown in Fig. 3. The subtype of acute encephalitis was as follows: 10 patients with HSE, 12 patients with NHALE, 4 patients with paraneoplastic encephalitis, 2 patients with encephalitis associated with collagen disease, one case of viral encephalitis other than HSE and 20 patients with encephalitis with unknown causes.

Clinical features of NHALE patients in Tottori Prefecture

Twelve patients (five male patients and seven female patients) were reported as NHALE in this survey. The average onset age of NHALE patients in men was 44.8 ± 10.8 years and in women was 31.6 ± 8.3 years. Trends of incidence of NHALE by year or by month

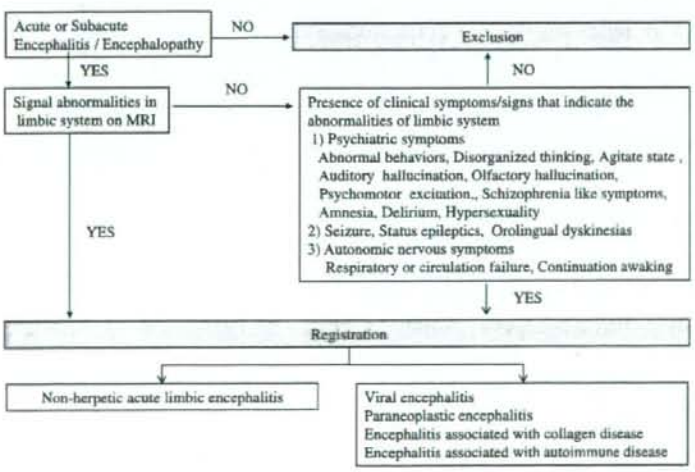

Figure 2 Flow chart of criteria for case registration of limbic encephalitis.

Table 1 Incidence of acute encephalitis patients from 2001 to 2005

	Male + Female		Male		Female	
Age (years)	*n*	Incidence rate	*n*	Incidence rate	*n*	Incidence rate
≥16 (total)	49	19.0	30	24.7	19	14.0
16–19	2	13.4	0	–	2	27.7
20–29	10	29.6	5	29.0	5	30.2
30–39	8	22.6	6	34.1	2	11.3
40–49	9	23.2	4	20.7	5	25.7
50–59	5	11.1	5	22.0	0	–
60–69	4	10.9	1	5.9	3	15.3
70–79	9	26.8	8	56.7	1	5.1
≥80	2	10.5	1	17.6	1	7.4

Incidence rate per million person-years.

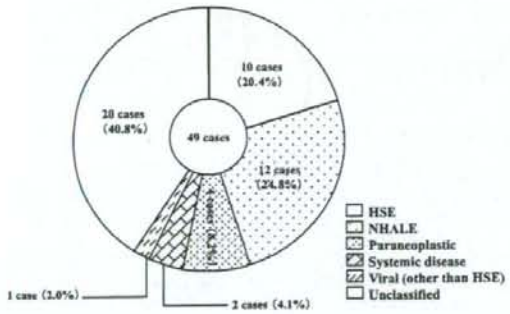

Figure 3 Subtypes of acute encephalitis. Number and percentage of subtypes of acute encephalitis are shown.

are shown in Fig. 4. In this area, at least one NHALE patient appeared every year. There were no patients who developed NHALE during the winter season from November to February. The incidence of NHALE patients is shown in Table 2. The incidence rate of adult patients with NHALE was calculated to be 4.7 (95%CI = 2.6–7.6) per million person-years. Examining 10-year groups, the highest incidence rate of NHALE patients was in 20-year-old females (24.2 per million person-years).

On the other hand, our survey identified 10 patients (five male and five female patients) with HSE. The incidence rate of adult patients with HSE was calculated to be 3.9 per million person-years (95%CI = 2.1–7.1). The average onset age of HSE patients was 54.1 ± 22.1 years. The incidence of NHALE patients was the same as that of HSE patients, but the average onset age of NHALE patients was lower than that of HSE patients. Finally, based on our results, around 550 new NHALE patients would appear every year in Japan.

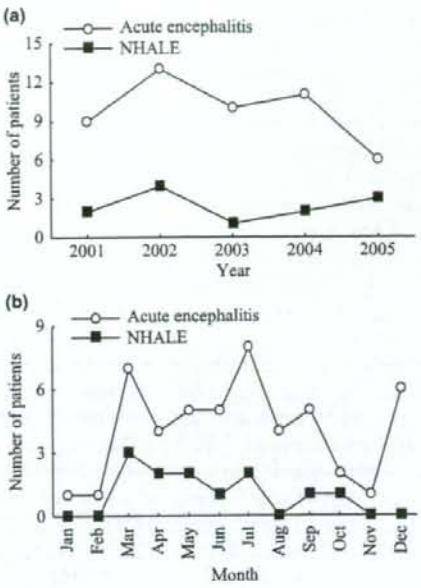

Figure 4 The number of non-herpetic acute limbic encephalitis (NHALE) patients by year or month. (a) At least one NHALE patient appeared per year in this area. (b) NHALE patients did not appear in the winter seasons in this area.

Table 2 Incidence of non-herpetic acute limbic encephalitis patients from 2001 to 2005

	Male + Female		Male		Female	
Age (years)	*n*	Incidence rate	*n*	Incidence rate	*n*	Incidence rate
≥16 (total)	12	4.7	5	4.1	7	5.1
20–29	4	11.8	0	–	4	24.2
30–39	3	8.5	2	11.4	1	5.7
40–49	2	7.8	1	5.2	2	10.3
50–59	2	4.4	2	8.8	0	–

Incidence rate per million person-years.

Discussion

In recent years, acute encephalitis of unknown aetiology that predominantly affects the limbic system has been increasingly recognized in Japan. Whilst reports of NHALE have rapidly increased in Japan, the incidence of patients with NHALE has not been examined. We conducted a questionnaire survey of acute encephalitis focusing on NHALE. It is difficult to estimate the incidence of acute encephalitis, because the diagnosis of encephalitis requires serial and extensive examination of the pathogens. To estimate the actual number of acute

